AGU ADVANCING EARTH AND SPACE SCIENCES

Water Resources Research

RESEARCH ARTICLE
10.1029/2024WR038450

A Generalized Framework to Describe Unimodal and Bimodal Soil Hydraulic Properties Over Full Water Saturation Range

Yunquan Wang[1], **Rui Ma**[1], **and Harry Vereecken**[2]

[1]Hubei Key Laboratory of Yangtze Catchment Environmental Aquatic Science, School of Environmental Studies, China University of Geosciences, Wuhan, China, [2]Agrosphere Institute, IBG-3, Forschungszentrum Jülich GmbH, Jülich, Germany

Key Points:

- A novel framework was proposed for describing unimodal and bimodal Soil hydraulic properties (SHPs) over the entire moisture range
- The framework takes into account the effects of soil structure, capillarity, adsorption forces, and vapor diffusion
- In its five free-fitted parameters form, the proposed models can capture both bimodal SWRCs and HCCs

Supporting Information:

Supporting Information may be found in the online version of this article.

Correspondence to:

Y. Wang,
wangyq@cug.edu.cn

Citation:

Wang, Y., Ma, R., & Vereecken, H. (2025). A generalized framework to describe unimodal and bimodal soil hydraulic properties over full water saturation range. *Water Resources Research*, *61*, e2024WR038450. https://doi.org/10.1029/2024WR038450

Received 17 JUL 2024
Accepted 20 JAN 2025

Abstract Soil hydraulic properties (SHPs) are impacted by various mechanisms such as soil structure, capillarity, and adsorption forces, often showing a bimodal shape. Developing soil hydraulic models (SHMs) that describe SHPs over the entire saturation range often involves balancing the representation of multiple processes while minimizing the number of free-fitted parameters. Existing SHMs rarely capture bimodal SHPs across the full moisture range or introduce a higher number of free-fitted parameters. In this study, we propose a novel framework to describe SHPs over the entire moisture range, accounting for the effects of soil structure, capillarity, adsorption forces, and vapor diffusion. In its four free-fitted parameters form, the proposed models can capture unimodal soil water retention curves and bimodal hydraulic conductivity curves (HCC). This model is well-suited for situations where small changes in water content near saturation are no longer detectable via measured SWRC, yet soil structure still causes a sharp decline in HCC near saturation. With one additional free-fitted parameter, the proposed models can capture both bimodal SWRC and HCC. Testing with 355 and 52 soil samples from two public datasets demonstrated that the proposed models performed exceptionally well in describing SHPs across the entire moisture range. The reported lowest root-mean-square error values were 0.005 and 0.009 cm^3 cm^{-3} for fitting SWRCs, and 0.465 and 0.666 for predicting HCCs, respectively. Due to the minimal introduction of free-fitted parameters, the proposed framework showed significant application potential.

1. Introduction

Soil hydraulic properties, including the soil water retention curve (SWRC) and hydraulic conductivity curve (HCC), are essential inputs for various soil water-related processes. Accurately describing and predicting SHPs is crucial for capturing water and solute transport at the field scale and for modeling the global water and energy cycle through land surface models (Clark et al., 2015; Fatichi et al., 2020; Gutmann & Small, 2007; Vereecken et al., 2022). The precise characterization of these properties is fundamental in hydrological modeling, irrigation management, and environmental protection, as they influence infiltration, runoff, and groundwater recharge (Fatichi et al., 2020; Seneviratne et al., 2010; Vereecken et al., 2016; Šimůnek et al., 2016). Additionally, reliable SHPs are vital for predicting the movement of nutrients and contaminants in soil, thereby contributing to better agricultural productivity and environmental sustainability (Madejón et al., 2019; Pinheiro et al., 2019; Vogel & Roth, 2003; Šimůnek & Genuchten, 2008).

Classical soil hydraulic models (SHMs) typically conceptualize soil pores as a series of capillaries of varying sizes, which can either be fully filled with water or completely emptied depending on the matric potential (Childs & Collis-George, 1950; Mualem, 1976a; Tuller & Or, 2001; van Genuchten, 1980). The pore size of these capillaries is related to matric potential through the Young-Laplace equation, which in turn relates to the SWRC (Mualem, 1976a; van Genuchten, 1980). However, when these capillary-based models are widely applied, their limitations become apparent.

In real soil, water can still exist in the corners of pores, retained by capillary forces (Tuller et al., 1999) and on the surfaces of soil particles, held by adsorption forces (Tuller et al., 1999; Tuller & Or, 2001; Yu & Wardlaw, 1986). These forms of water are neglected in classical SHMs but have been shown to significantly contribute to soil water flow, especially under dry conditions (e.g., Nimmo, 1991; Rossi & Nimmo, 1994; Tuller & Or, 2001; Wang et al., 2013). Consequently, classical SHMs tend to overestimate soil water content while underestimate hydraulic conductivity in the dry range (Lebeau & Konrad, 2010; Wang et al., 2016; Zhang, 2011). Additionally, these

models do not adequately account for the effects of soil structure, particularly the presence of macropores (van Genuchten & Nielsen, 1985; Schaap & Leij, 2000; Schaap et al., 2001). In macropores, water movement is mainly influenced by gravitational forces rather than capillary forces (Gerke, 2006). Therefore, applying the Young-Laplace equation to describe the relationship between pore diameter and matric potential is not appropriate for macropores. Furthermore, the influence of macropores occurs within a narrow range of matric potentials, such as 0 to −6 cm (Jarvis, 2007). Conventional methods for measuring the SWRC often fail to capture soil structure information. As a result, classical SHMs tend to overestimate hydraulic conductivity in the medium water content range when using saturated hydraulic conductivity (K_s) as a matching point (van Genuchten & Nielsen, 1985; Schaap & Leij, 2000; Schaap et al., 2001; Wang et al., 2023).

In terms of the effects of adsorption forces, early improvements primarily focused on the SWRC (Campbell & Shiozawa, 1992; Du, 2020; Fayer & Simmons, 1995; Khlosi et al., 2006; Lu et al., 2008; Morel-Seytoux & Nimmo, 1999; Nimmo, 1991; Rooij et al., 2021; Rossi & Nimmo, 1994; Webb, 2000; Zheng et al., 2020). These proposed models generally introduced a correction or scaling factor to ensure the residual water content of capillarity-based model goes to zero at a matric potential of about -10^7 cm. One exception is the work by Fredlund and Xing (1994), who introduced a correction factor that affects the entire moisture range, rather than being limited to the residual water content. Tuller et al. (1999) and Tuller and Or (2001) introduced a novel framework to incorporate the effects of both capillarity and adsorption forces on both SWRC and HCC. They developed different functions to describe the SHPs in relation to water retained in completely filled pores, in pore corners, and on the surfaces of soil particles. Subsequently, Lebeau and Konrad (2010) integrated the entire model by combining an existing capillary model with a film model. They utilized the Kosugi (1994, 1996) model for describing SHPs that account for capillary forces and employed the Campbell and Shiozawa (1992) model and Tokunaga (2009) model for describing the SWRC and HCC to account for adsorption forces, respectively. Notably, through building a physical relationship between the film conductivity and the SWRC in the dry range, the model proposed in Lebeau and Konrad (2010) does not require additional free-fitted parameter to describe the SHPs in relation to adsorption forces. Following works that take into the effects of adsorption forces rarely go beyond the framework developed by Lebeau and Konrad (2010). This combination method was further applied by Zhang (2011), Peters (2013), and many others, with variations primarily in the choice of capillary models to represent the effects of capillarity and the construction of different SWRCs to account for the effects of adsorption forces (e.g., Liao et al., 2018; Stanić et al., 2020; Wang et al., 2016; Weber et al., 2019; Yang et al., 2023). To minimize the number of free-fitted parameters, subsequent studies have employed methods similar to those used by Lebeau and Konrad (2010) to estimate the saturated film hydraulic conductivity from the SWRC in the dry range (Peters et al., 2021; Wang et al., 2017). As a rare exception, Wang et al. (2018) reconstructed the saturation term based on the SWRC proposed by Fredlund and Xing (1994) and developed a continuous HCC formula similar to the Mualem-type conductivity function (de Rooij, 2024). This formula captures the effects of both capillary and adsorption forces without requiring additional formulations to describe SHPs related to adsorption forces. More recently, Wang, Ma, and Zhu (2022) and Peters et al. (2023) proposed methods for predicting absolute hydraulic conductivity from a known SWRC without requiring knowledge of K_s. Specifically, Wang, Ma, and Zhu (2022) used the estimated hydraulic conductivity in the dry range as a new matching point, while Peters et al. (2023) introduced an empirically derived saturated tortuosity parameter to estimate unsaturated hydraulic conductivity. Both models demonstrated superior performance compared to the traditional approach, which uses K_s as a matching point. Notably, water retained in corners was specifically addressed in Tuller et al. (1999) and in Diamantopoulos and Durner (2013), whereas in other above-mentioned studies, this aspect is often either omitted or represented empirically.

In terms of the effects of soil structure, including the presence of macropores near saturation and the bimodal (or even multimodal) distribution of pore size, several solutions have been proposed. One method focuses primarily on the HCC, using both K_s and an additional saturated matrix hydraulic conductivity to represent the effects of soil structure and soil matrix, respectively (e.g., Børgesen et al., 2006; Jarvis et al., 1991; Larsbo et al., 2005; Schaap & Van Genuchten, 2006). Another approach considers the effects of soil structure on both the SWRC and HCC by using a sum of two classical SHMs to capture bimodal SHPs (Durner, 1994; Othmer et al., 1991; Romano et al., 2011; Ross & Smettem, 1993; Zhang et al., 2022). Although these bimodal SHMs are widely accepted in the literature, they come with the cost of introducing two to three more free-fitted parameters than classical SHMs, complicating their application.

Despite solutions being developed for each of the above-mentioned shortcomings, few existing SHMs address all these issues together. A recent work by Wang et al. (2023) proposed a third version of the Fredlund and Xing (1994)-Wang et al. (2018) model (named as the FXW-M3 model hereafter), considering the effects of soil structure near saturation, capillary forces, and adsorption forces. However, it cannot describe the influence of soil structure due to a bimodal particle size distribution. Applying a traditional bimodal framework similar to the Durner (1994) model comes at the cost of introducing a larger number of free-fitted parameters. Additionally, the capillary conductivity in the FXW-M3 model is represented by an essentially empirical approach, which introduces a level of uncertainty to the model's performance (Wang et al., 2018).

Therefore, in this study, we developed a novel framework to describe SHPs over the entire moisture range, taking into account the effects of soil structure, capillary forces, adsorption forces, as well as vapor diffusion. In its unimodal SWRC form, the model has the same number of free-fitted parameters as the classic capillarity-based models, such as the van Genuchten (1980)-Mualem (1976a) model (VGM model hereafter). In its bimodal SWRC form, it requires only one additional free-fitted parameter compared to its unimodal model counterpart.

2. Model Development

2.1. The Generalized Framework for Describing Unimodal and Bimodal Soil Water Retention Curves

The main difference between the classical SWRC that accounts for capillary forces and an SWRC that additionally accounts for adsorption forces lies in the behavior of soil water content as the matric potential approaches h_0, the matric potential at zero soil water content. Classical models often fail to predict the soil water content accurately at very low matric potentials, where adsorption forces become significant. To address this, we introduce a scaling factor $C(h)$, similar to the approach of Fredlund and Xing (1994), which modifies the SWRC to ensure that soil water content approaches zero as the matric potential approaches h_0. The new SWRC can be expressed as:

$$\theta = C(h)[(\theta_s - \theta_r)\Gamma(h) + \theta_r] \tag{1}$$

where θ ($L^3\ L^{-3}$) is the volumetric water content; θ_s ($L^3\ L^{-3}$) and θ_r ($L^3\ L^{-3}$) are the saturated and the residual water content, respectively; $\Gamma(h)$ is the saturation degree that accounts for capillary forces and could be expressed by any existing models. Here, we evaluate three widely applied capillary models: the van Genuchten (1980) model, the Kosugi (1994) model and the Fredlund and Xing (1994) model (Table 1). Notably, when applying the Fredlund and Xing (1994) model for $\Gamma(h)$, θ_r is set to zero.

Meanwhile, the introduced $C(h)$ function should have the flexibility to capture the second modal characteristic of the SWRC. Together with the capillary saturation function $\Gamma(h)$, which captures the first modal property, Equation 1 can now capture the bimodal shape of the SWRC. To meet these requirements, the scaling function $C(h)$ is defined as:

$$C(h) = \left[1 - \frac{\ln(1 + h/h_r)}{\ln(1 + h_0/h_r)}\right]^{n_c} \tag{2}$$

where h_r is a shape parameter assigned a value of -1.5×10^4 cm (Fredlund & Xing, 1994); h_0, which corresponds to a water content of zero, is set to -6.3×10^6 cm (Schneider & Goss, 2012); and n_c is a shape parameter. When n_c equals 1, Equation 2 returns to the same form proposed by Fredlund and Xing (1994), making Equation 1 suitable for describing unimodal SWRC. In contrast, when n_c is treated as a free-fitted parameter, Equation 1 has the flexibility to describe bimodal SWRC.

2.2. The Generalized Framework for Describing Hydraulic Conductivity Curves

The overall hydraulic conductivity K is a sum of each component, which accounts for the effects of soil structure, capillary forces, adsorption forces, as well as vapor diffusion. This can be expressed as (Peters, 2013):

$$K = K_c + K_f + K_v \tag{3}$$

Table 1
The Closed-Form Equations for Different SWRCs

Model	$\Gamma(h)$	$F(h)$
U-VGM model	$[1 + \lvert\alpha h\rvert^n]^{-m}$	$1 - \left(1 - \Gamma(h)^{1/m}\right)^m$
U-Ko model	$0.5erfc\left(\frac{\ln(h/h_{median})}{\sqrt{2}\delta}\right)$	$0.5erfc\left(\frac{\ln(h/h_{median})}{\sqrt{2}\delta} + \frac{\delta}{\sqrt{2}}\right)$
U-FXW model	$[\ln(e + \lvert\alpha h\rvert^n)]^{-m}$	$1 - \left(1 - \Gamma(h)^{1/m}\right)^{1-1/n}$

Note. U-VGM, U-Ko and U-FXW refers to the proposed unimodal-SWRC model that applying the van Genuchten (1980)-Mualem (1976a) model, the Kosugi (1994) model and the Fredlund and Xing (1994)-Wang et al. (2018) model for describing the capillarity-associated soil hydraulic properties, respectively.

where K_c is the hydraulic conductivity that accounts for the effects of capillary forces as well as soil structure, K_f and K_v are the hydraulic conductivities that accounts for the effects of adsorption forces and vapor diffusion, respectively.

2.2.1. K_c

2.2.1.1. Unimodal-Soil Water Retention Curve Model

When $n_c = 1$, the effects of $C(h)$ are generally neglected in the matric potential range where capillarity dominates (Wang et al., 2016). Substituting $\Gamma(h)$ into Mualem's (1976a) model results in the expression for K_c, which can be written as:

$$K_c = K_s\Gamma(h)^l\left[\frac{F(h)}{F(0)}\right]^2 \tag{4}$$

where l is a parameter that accounts for tortuosity and connectivity, $F(h)$ is described as:

$$F(h) = \int_{\Gamma(h_0)}^{\Gamma(h)}\frac{1}{h}d\Gamma \tag{5}$$

However, since the effects of macropores occur in a narrow matric potential range and are generally not captured in SWRC measurements, using K_s as the matching point, as in Equation 4, tends to overestimate the unsaturated hydraulic conductivity. To address this, we applied the model developed in Wang et al. (2023) to better capture the effects of macropores. The expression for K_c is further described as:

$$K_c(h) = \begin{cases} K(h_a)\left(\frac{\Gamma(h)}{\Gamma(h_a)}\right)^l\left[\frac{F(h)}{F(h_a)}\right]^2 & h < h_a \\ K_s\Gamma(h)^{\frac{\ln(K(h_a)/K_s)}{\ln(\Gamma(h_a))}} & h \geq h_a \end{cases} \tag{6}$$

where h_a is the critical matric potential that separates the effects of soil structure and soil matrix. The value of h_a is set to −6 cm, following Jarvis (2007). K (h_a) is the corresponding hydraulic conductivity, known as the saturated matrix hydraulic conductivity (Børgesen et al., 2006; Jarvis et al., 1991; Larsbo et al., 2005; Peters et al., 2023; Wang et al., 2023).

When applying the van Genuchten (1980) model and the Kosugi (1994) model for describing $\Gamma(h)$, the closed-form expression of $F(h)$ can be easily derived (Table 1). In contrast, when applying the Fredlund and Xing (1994) model for describing $\Gamma(h)$, no closed-form expression of $F(h)$ exists. Here, we apply the empirical HCC derived by Wang et al. (2018, 2023) to describe the hydraulic conductivity that accounts for both capillary and adsorption forces when applying the Fredlund and Xing (1994) model (Appendix A).

2.2.1.2. Bimodal-Soil Water Retention Curve Model

When treating n_c as a free-fitted parameter, however, the impact of $C(h)$ is no longer negligible at low water content values, and K_c needs to be derived numerically. Mualem's (1976a) model was described as

$$K_c(h) = \begin{cases} K(h_a)\left(\frac{S(h)}{S(h_a)}\right)^l\left[\frac{F(h)}{F(h_a)}\right]^2 & h < h_a \\ K_sS(h)^{\frac{\ln(K(h_a)/K_s)}{\ln(S(h_a))}} & h \geq h_a \end{cases} \tag{7}$$

where $S = \theta/\theta_s$. The integration formula $F(h)$ was expressed as

$$\begin{aligned} \mathrm{F}(h) &= \int_{S(h_0)}^{S(h)} \frac{1}{h} dS = \int_{h_0}^{h} \frac{1}{h} \frac{dS}{dh} dh \\ &= \frac{1}{\theta_s} \int_{h_0}^{h} \frac{1}{h} [(\theta_s - \theta_r)\Gamma(h) + \theta_r] \frac{dC(h)}{dh} dh + \frac{1}{\theta_s} \int_{h_0}^{h} \frac{1}{h} (\theta_s - \theta_r)\, C(h) \frac{d\Gamma(h)}{dh} dh \end{aligned} \tag{8}$$

Equation 8 needs to be solved numerically. Notably, for the bimodal model, we also introduce the parameter of $K(h_a)$ to describe the effects of soil structure. This is because the effects of soil structure near saturation are seldom captured in the measured SWRC (Zhang et al., 2022).

2.2.2. K_f

The film conductivity is controlled by the specific surface area and the film thickness (Lebeau & Konrad, 2010; Tokunaga, 2009). Following the scaling method applied in Wang et al. (2016), K_f can be expressed as

$$K_f(h) = (1 - \Gamma(h))\, K_f(h_m) \left(\frac{h}{h_m}\right)^{-1.5} \tag{9}$$

where h_m is a typical matric potential dominated by van der Waals forces, set to -1.0×10^5 cm following Lebeau and Konrad (2010). According to Wang, Zhou, et al. (2022), the corresponding hydraulic conductivity $K_f(h_m)$ can be derived from the SWRC in the dry range, expressed as:

$$K_f(h_m) = b\theta_m \tag{10}$$

where b represents the combined effects of film thickness, specific surface area, and a correction factor on conductivity estimation, as described by Wang, Ma, and Zhu (2022). According to Wang, Zhou, et al. (2022), b has a value of 4.062×10^{-6} cm d^{-1}. For a detailed estimation of b and $K_f(h_m)$, please refer to Wang, Zhou, et al. (2022).

2.2.3. K_v

For very dry conditions, vapor diffusion also contributes to the overall hydraulic conductivity. Here, following Saito et al. (2006), the isothermal conductivity of vapor flow is expressed as:

$$K_v = \frac{\rho_v}{\rho} D_v \frac{Mg}{RT} RH \tag{11}$$

where ρ_v (kg m^{-3}) and ρ (kg m^{-3}) denotes the saturated vapor density and the liquid density of water, respectively. M is the molecular mass of water (0.018015 kg mol^{-1}), g is the gravitational acceleration (9.81 m s^{-2}), R is the universal gas constant (8.314 J mol^{-1} K^{-1}), and T is the Kelvin temperature (set as 293.15 K). RH is the relative humidity, which can be estimated by the Kelvin equation, written as

$$RH = \exp\left(\frac{hMg}{RT}\right) \tag{12}$$

where h (m) is the matric potential.

D_v (m^2 s^{-1}) represents the vapor diffusivity in soil, given by:

$$D_v = \tau\theta_a D_a = \frac{\theta_a^{10/3}}{\theta_s^{2}} D_a \tag{13}$$

where θ_a is the air-filled porosity, τ is the tortuosity factor calculated according to Millington and Quirk (1961), and D_a (m^2 s^{-1}) is the vapor diffusivity in air, calculated as:

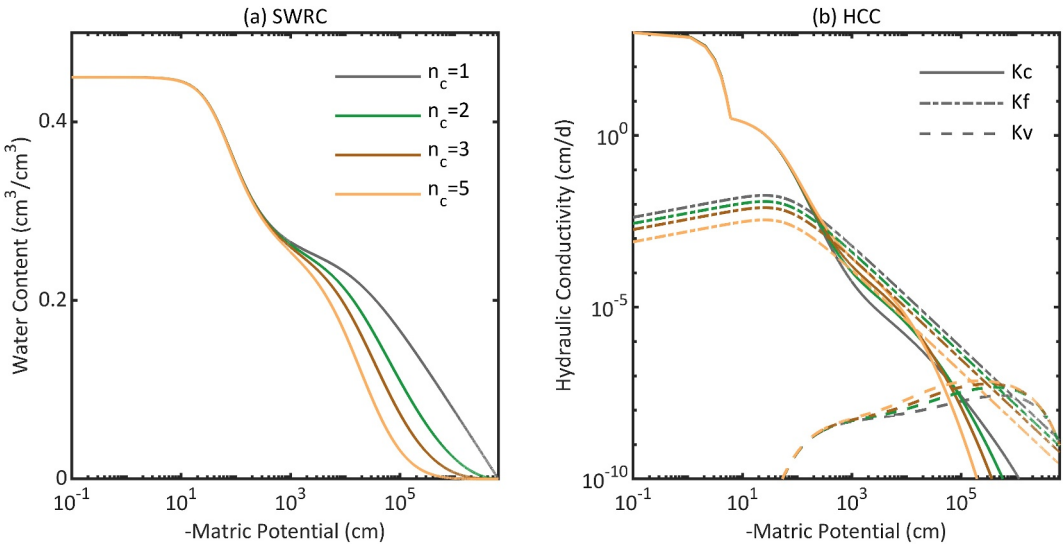

Figure 1. Illustration of the new framework with van Genuchten (1980) model applied for $\Gamma(h)$. K_c, K_f and K_v represents the hydraulic conductivity that accounts for capillarity, adsorption forces and vapor diffusion, respectively. Parameters setting are: $\theta_r = 0.25$ cm^3 cm^{-3}, $\theta_s = 0.45$ cm^3 cm^{-3}, $\alpha = 0.02$ cm^{-1}, $n = 1.8$, $K_s = 10^3$ cm d^{-1}, $K(h_a) = 10^{0.5}$ cm d^{-1}.

$$D_a = 2.12 \times 10^{-5} \left(\frac{T}{273.15} \right)^2 \tag{14}$$

Figure 1 shows the impact of different n_c on SWRC and HCC. The van Genuchten (1980) model was applied for $\Gamma(h)$. Notably, when n_c is kept constant at 1, Equation 1 can describe bimodal characteristics in certain cases (Figure 1a), but it lacks the flexibility to accurately capture bimodal SWRC in most scenarios, as evidenced in the results section. In contrast, when n_c is treated as a free-fitted parameter, Equation 1 can capture bimodal SWRC (Figure 1a). The higher the value of n_c, the sharper the decrease in soil water content in the dry range. The impact of n_c on the overall HCC is restricted in the range where the water content is less than θ_r. The direct impact is on K_c, which has a higher value for higher n_c when the water content is close to θ_r. In contrast, when the water content is very low, K_c has a smaller value for higher n_c. The reason is that a higher n_c value indicates a smaller portion of film water held by adsorption forces (Figure 1a). Consequently, the water retained by capillarity—the difference between total water content and film water—is higher when the water content is close to θ_r, but smaller under very dry conditions. n_c indirectly affects K_f and K_v by influencing the soil water content in the dry range. The higher the n_c, the lower the soil water content in the dry range (Figure 1a), resulting in a smaller K_f according to Equation 10. Simultaneously, the lower the soil water content, the larger air-filled porosity, leading to a larger K_v according to Equations 11 and 13. Additionally, the introduction of $K(h_a)$ results in a bimodal HCC in the wet range.

The classic framework for describing bimodal SWRC typically requires at least two to three additional free-fitted parameters compared to unimodal model (Durner, 1994). In contrast, the new bimodal SWRC developed here requires only one additional free-fitted parameter of n_c. This efficiency is achieved by the careful selection and definition of the scaling factor, which incorporates the bimodal characteristics without excessively increasing the model's complexity.

3. Materials and Methods

3.1. Data Sets

The datasets applied in this study come from Hohenbrink et al. (2023). To incorporate more information near saturation, and following Wang et al. (2023), we require the measured $\theta(h)$ should have at least two data pairs at matric potentials higher than −10 cm. However, only a few soil samples from Hohenbrink et al. (2023) provide detailed HCC measurements near saturation. We require the measured K_s is provided to predict the HCC from the SWRC. Consequently, a total of 355 soil samples were selected from the Hohenbrink et al. (2023) dataset.

Notably, through the combined usage of the evaporation method and the dewpoint method, the measured SHPs in Hohenbrink et al. (2023) cover a wide saturation range, making them well-suited for evaluation. Readers are referred to Hohenbrink et al. (2023) for detailed information.

In addition to the Hohenbrink et al. (2023) dataset, we also selected 52 soil samples from the UNsaturated SOil hydraulic database (UNSODA) (Nemes et al., 2001) as an independent data source to evaluate the model performance. These 52 soil samples were also utilized in Wang et al. (2023) and meet the following criteria: the measured $\theta(h)$ should have at least two data pairs at matric potentials higher than -10 cm; the measured $K(h)$ dataset should include K_s and at least two additional data points at matric potentials higher than -20 cm. Additionally, both $\theta(h)$ and $K(h)$ should have at least five measured data points.

This independent dataset allows for a more robust validation of the model across different soil types and conditions, ensuring its general applicability and reliability.

3.2. Optimization Procedure

To enable the proposed model to predict HCC from SWRC with known K_s, as widely applied in the literature, we optimize the parameters of SWRC and HCC separately.

First, Equation 1 was optimized with observed SWRC to derive the parameters. The objective function $\Phi_\theta(p)$ to be minimized is defined as:

$$\Phi_\theta(p) = \sum_{i=1}^{n_\theta} \left[\theta_i - \overline{\theta}_i(p)\right]^2 \tag{15}$$

where n_θ is the number of data pairs for the retention; and θ_i and $\overline{\theta}_i$ are the measured and the fitted water content, respectively. p is the parameter vector used for the optimization. For example, $p = (\alpha, n, \theta_r, \theta_s)$ and $p = (\alpha, n, \theta_r, \theta_s, n_c)$ for the U-VGM and B-VGM model, respectively.

Second, with the parameter vector p determined, Equation 3 was optimized with observed HCC to derive the parameter of K (h_a). The optimization function $\Phi_K(K(h_a))$ is defined as

$$\Phi_K(K(h_a)) = \sum_{i=1}^{n_K} \left[\log_{10}\left(\frac{K_i}{\overline{K}_i(K(h_a))}\right)\right]^2 \tag{16}$$

where n_K is the number of data pairs for the HCC; and K_i and $\overline{K}_i$ are the measured and the fitted hydraulic conductivity, respectively.

The optimization process utilized the shuffled complex evolution method, a well-established optimization technique developed by Duan et al. (1992) at the University of Arizona (the SCE-UA method). In this method, the number of complexes used for the optimization search was set to match the number of optimized parameters. Additionally, the maximum number of allowed trials was set to 20,000, and the number of shuffling loops was set to 20. The other parameters are set as recommended.

We have listed all the optimized and fixed parameters for different model settings in Table 2.

To evaluate the model performance, the root-mean-square error ($RMSE$) is defined as:

$$RMSE = \sqrt{\frac{1}{N}\sum_{i=1}^{N}(o_i - \overline{o}_i)^2} \tag{17}$$

where N represents the number of data pairs; and o_i and $\overline{o}_i$ are the measured and estimated values, respectively. In terms of conductivity, the $\log_{10}(K)$ value is applied.

R^2 is defined as:

Table 2
The Optimized and Fixed Parameters of Different Model Settings

Model	Optimized parameters	Fixed parameters
U-VGM/B-VGM	α (0.001, 0.5), cm^{-1} n (1.0, 15) θ_r (0.0, 0.5) θ_s (0.2, 0.9) n_c (1, 15) K (h_a) (0.01, 10^4), cm d^{-1}	$l = 0.5$ K_s $b = 4.062 \times 10^{-6}$ cm d^{-1} $h_a = -6.0$ cm $h_m = -1.0 \times 10^5$ cm $h_r = -1.5 \times 10^4$ cm $h_0 = -6.3 \times 10^6$ cm
U-Ko/B-Ko	h_{median} (1.0, 10^4), cm δ (0.001, 15) θ_r (0.0, 0.5) θ_s (0.2, 0.9) n_c (1, 15) K (h_a) (0.01, 10^4), cm d^{-1}	$l = 0.5$ K_s $b = 4.062 \times 10^{-6}$ cm d^{-1} $h_a = -6.0$ cm $h_m = -1.0 \times 10^5$ cm $h_r = -1.5 \times 10^4$ cm $h_0 = -6.3 \times 10^6$ cm
U-FXW/B-FXW	α (0.001, 0.2), cm^{-1} n (1.01, 15) m (0.01, 1.5) θ_s (0.20, 0.9) n_c (1, 15) K (h_a) (0.01, 10^4), cm d^{-1}	$l = 3.5$ for U-FXW/$l = 0.5$ for B-FXW K_s $b = 4.062 \times 10^{-6}$ cm d^{-1} for B-FXW $h_a = -6.0$ cm $h_m = -1.0 \times 10^5$ cm $h_r = -1.5 \times 10^4$ cm $h_0 = -6.3 \times 10^6$ cm

Note. B-VGM, B-Ko and B-FXW refers to the proposed bimodal-SWRC model that applying the van Genuchten (1980)-Mualem (1976a) model, the Kosugi (1994) model and the Fredlund and Xing (1994)-Wang et al. (2018) model for describing the capillarity-associated soil hydraulic properties, respectively. The number in the bracket demonstrates the lower and upper boundary of the optimized parameters. Notably, n_c is only optimized for the bimodal models.

$$R^2 = \frac{\left(\sum_{i=1}^{N}(x_i - \overline{x})(y_i - \overline{y})\right)^2}{\sum_{i=1}^{N}(x_i - \overline{x})^2 \sum_{i=1}^{N}(y_i - \overline{y})^2} \tag{18}$$

where $\overline{x}$ and $\overline{y}$ are the mean value of x_i and y_i, respectively.

We also employed the Akaike Information Criterion (AIC) (Akaike, 1974; Ye et al., 2008; Zhang et al., 2022) to determine the most suitable model while taking into account the number of parameters. The AIC measures the quality of a model by estimating the difference between the unknown true likelihood function of the data and the fitted likelihood function of the model being used. The fundamental idea of AIC is to balance model accuracy and simplicity when fitting data. A smaller AIC value indicates that the model achieves a better balance between goodness of fit and complexity. The AIC is calculated using the following equation:

$$AIC = N \ln\left(\frac{1}{N}\sum_{i=1}^{N}(o_i - \overline{o}_i)^2\right) + 2N_p \tag{19}$$

where N is the number of measured data pairs and Np is the number of free-fitted parameters.

3.3. Prediction of K (h_a) Using Regression Method

The introduction of K (h_a) is intended to differentiate the impacts of soil structure and soil matrix. K (h_a) is considered to be closely related to the shape of the SWRC. For instance, Wang et al. (2023) developed a physically based method to estimate K (h_a) from the SWRC. However, their method necessitates that the proposed model captures the effects of both capillary and adsorption forces on HCC in a continuous formula, a criterion not met by the model proposed in this study. To enable the proposed models to predict HCC from measured SWRC, we established a relationship between the fitted parameter K (h_a) and the fitted parameters of the SWRC using a simple regression method. Take the U-VGM model for example, K (h_a) is defined as

$$K(h_a) = \boldsymbol{x}(1) * (\theta_s - \theta_r)^{\boldsymbol{x}(2)} * \alpha^{\boldsymbol{x}(3)} * n^{\boldsymbol{x}(4)} * m^{\boldsymbol{x}(5)} \quad (20)$$

where $\boldsymbol{x}$ is the parameter vector used for the optimization.

To test the performance of Equation 19 in estimating $K(h_a)$, we randomly divided the 355 soil samples from Hohenbrink et al. (2023) into two sets: 70% for training and 30% for testing.

4. Results

4.1. Optimization Results

4.1.1. Unimodal Models

Figure 2 summarizes the optimized results of three unimodal models, tested with 355 soil samples. As shown, all three models generally perform well in terms of the SWRC, each reporting the same *RMSE* value of 0.008 $cm^3\ cm^{-3}$. However, when the observed water content is roughly less than about 0.3 $cm^3\ cm^{-3}$, all three models tend to overestimate the water content for some soil samples. In terms of the HCC, all three models show good agreement with observations across both wet and dry ranges. The *RMSE* values for HCC range from 0.222 for the U-FXW model to 0.257 for the U-Ko model. The R^2 values range from 0.928 for the U-Ko model to 0.945 for the U-FXW model.

These results indicate that while the models are effective in capturing the overall trends, there are still areas, particularly at lower water contents, where improvements could be made. Among the three unimodal models, the U-FXW model performs slightly better in describing SHPs when evaluating with the 355 soil samples from the Hohenbrink et al. (2023) dataset.

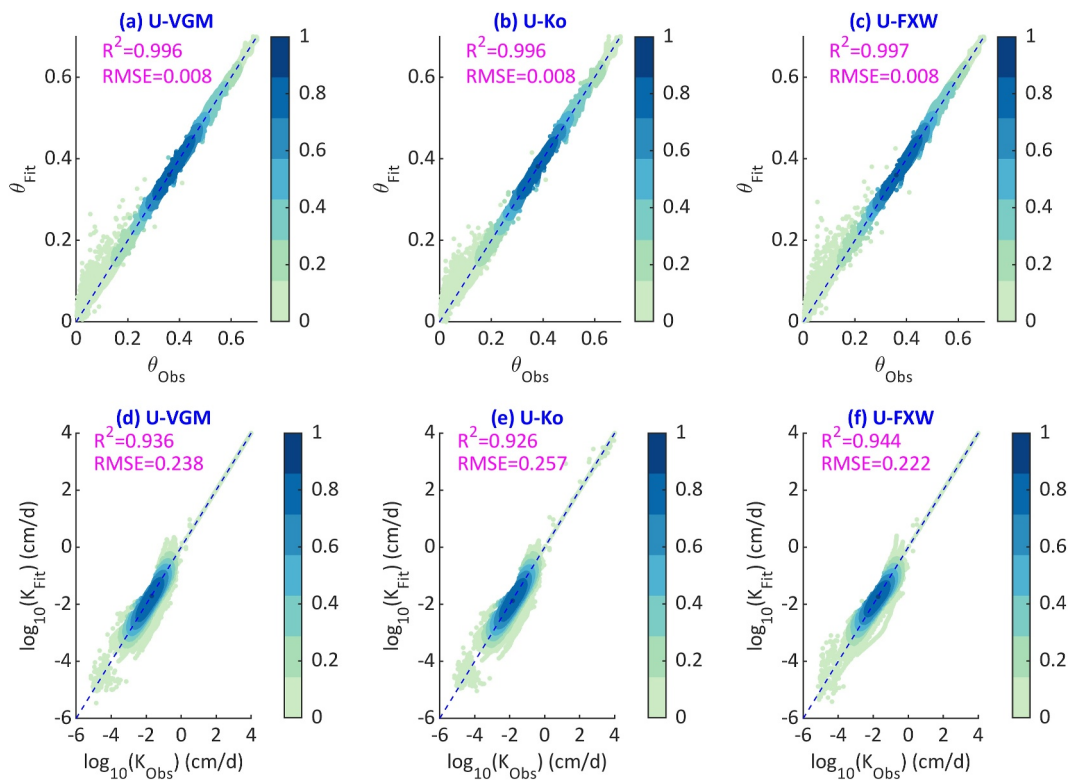

Figure 2. Optimized results of three unimodal models, testing with 355 soil samples from Hohenbrink et al. (2023). Panels (a) to (c) show the fitted SWRCs, while panels (d) to (f) show the fitted HCCs for the U-VGM, U-Ko, and U-FXW models, respectively.

4.1.2. Bimodal Models

Compared to the unimodal models, the bimodal models, with one additional free-fitted parameter, show much better performance, especially in fitting the SWRC as illustrated in Figure 3. The three bimodal models improve the model performance in dry range, the reported *RMSE* value is 0.005 cm^3 cm^{-3} for B-VGM and B-FXW models and is 0.006 cm^3 cm^{-3} for the B-Ko model. The values are much lower than the 0.008 cm^3 cm^{-3} of the three unimodal models. When it comes to the HCC, the B-FXW model shows the largest improvement, with *RMSE* being 0.190 and R^2 being 0.960, much lower and higher compared to the 0.222 and 0.945 of the U-FXW model. The B-VGM and B-Ko model only slightly improves the model performance compared to the U-VGM and U-Ko model, reducing the *RMSE* from 0.238 of U-VGM model and 0.257 of U-Bo model to 0.222 and 0.246, respectively. Among the three bimodal models, the B-FXW model performs the best in describing SHPs when evaluating with the 355 soil samples from the Hohenbrink et al. (2023) dataset.

Table 3 summarizes the percentage of individual soil samples where each model showed the best performance according to the calculated AIC values. When fitting SWRC alone, all three bimodal-SWRC models demonstrated superior performance over unimodal-SWRC models, with the lowest AIC values for more than 85% of soil samples. When considering both SWRC and HCC together, the bimodal-SWRC models performed better for over half of the soil samples. Among these models, the B-FXW model is the most recommended, as it exhibited the lowest AIC values for approximately 70% of the soil samples.

4.2. Parameters Analysis

4.2.1. Distribution of n_c

The distribution of n_c shows no clear patterns, as illustrated in Figure 4. For a given soil type, n_c can vary widely, especially in Sandy loam and Silty loam. For Sand, Sandy clay loam, Silt clay, and Clay, n_c generally varies within a narrow range for the three bimodal-SWRC models. For the B-VGM and B-Ko models, the fitted n_c has a similar distribution across different soil types except for Silt. In Silt, the B-VGM model has a relatively wide n_c

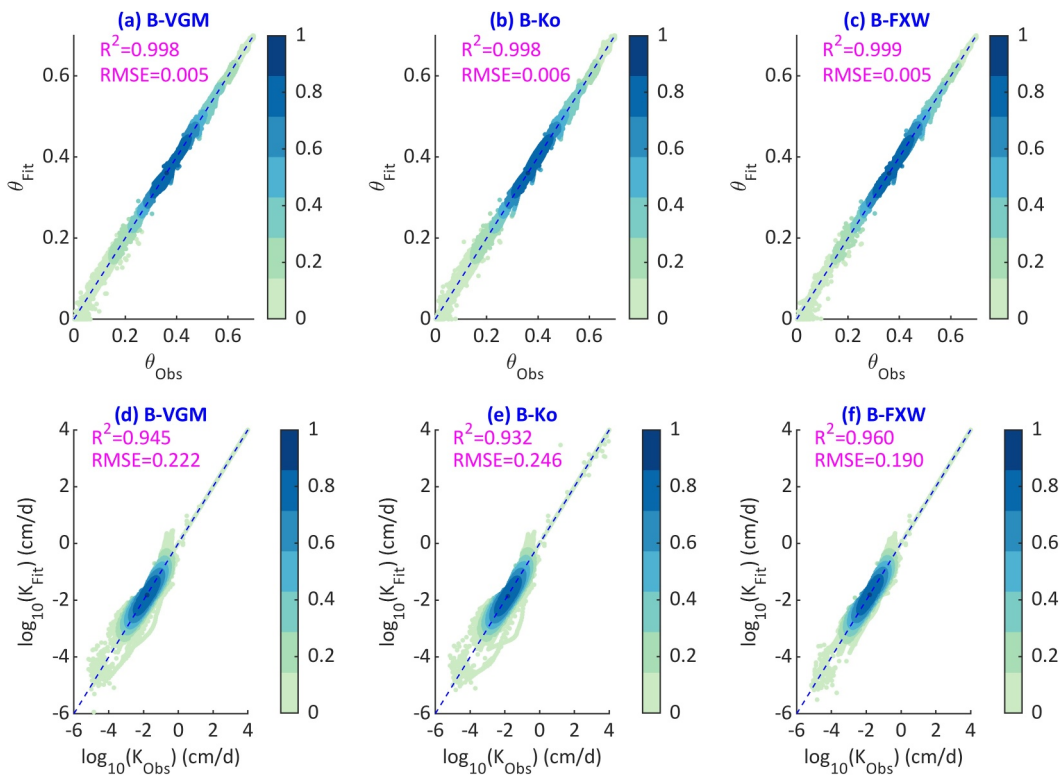

Figure 3. Optimized results of three bimodal models, testing with 355 soil samples. Panels (a) to (c) show the fitted SWRCs, while panels (d) to (f) show the fitted HCCs for the B-VGM, B-Ko, and B-FXW models, respectively.

Table 3
The Number and Percentages for the Best Model Between Unimodal and Bimodal-SWRC Models Identified by the Lowest Akaike Information Criterion Values

		Unimodal-SWRC models			Bimodal-SWRC models		
		U-VGM	U-Ko	U-FXW	B-VGM	B-Ko	B-FXW
$\theta(h)$	Total fits	47	47	44	308	308	311
	Percentage	13.2	13.2	12.4	86.8	86.8	87.6
$\theta(h) + K(h)$	Total fits	161	156	106	194	199	249
	Percentage	45.4	43.9	29.9	54.7	56.1	70.1

distribution and higher n_c values, while the B-Ko model shows a narrow distribution with smaller n_c values. The B-FXW model displays different n_c distributions for mainly Sand and Loamy sand. For instance, the mean value of the fitted n_c for the B-FXW model is about 1.5 for Sand, whereas it is around 15 for both the B-VGM and B-Ko models. For other soil types, the fitted n_c of the B-FXW model shows a similar distribution to the B-VGM and B-Ko models. The different n_c distributions across models could result from their distinct $\Gamma(h)$ expressions. Overall, the distribution of n_c exhibits no clear patterns and no obvious relationship with soil textures. Since the SWRC is also controlled by four other parameters, n_c is better interpreted as a shaping factor rather than having a clear physical meaning.

4.2.2. Distribution of K (h_a)

The fitted K (h_a) values are nearly identical across the three bimodal models. Using the B-FXW model, which exhibits the lowest *RMSE*, as an example, the distribution of the fitted K (h_a) is demonstrated in Figure 5a. The fitted K (h_a) values generally range from 1 cm d^{-1} to 100 cm d^{-1}. As the mean clay percentage increases across different soil types, the fitted mean K (h_a) value tends to decrease from Sand to Silty loam and then increase toward Silty clay. Clay reports the lowest K (h_a) values, with a mean value of less than 1 cm d^{-1}. In contrast, the observed K_S varies across a much wider range, from about 10 cm d^{-1} to 1.0×10^4 cm d^{-1}. Interestingly, for fine-textured soils with high clay content, the observed K_S is generally higher than that of coarse-textured soils. The K (h_a)/K_S ratio shows an overall decreasing trend for soil types with increased clay content, as shown in Figure 5c. The mean value of the K (h_a)/K_S ratio ranges from about 0.01 for Clay to about 0.5 for Loamy sand.

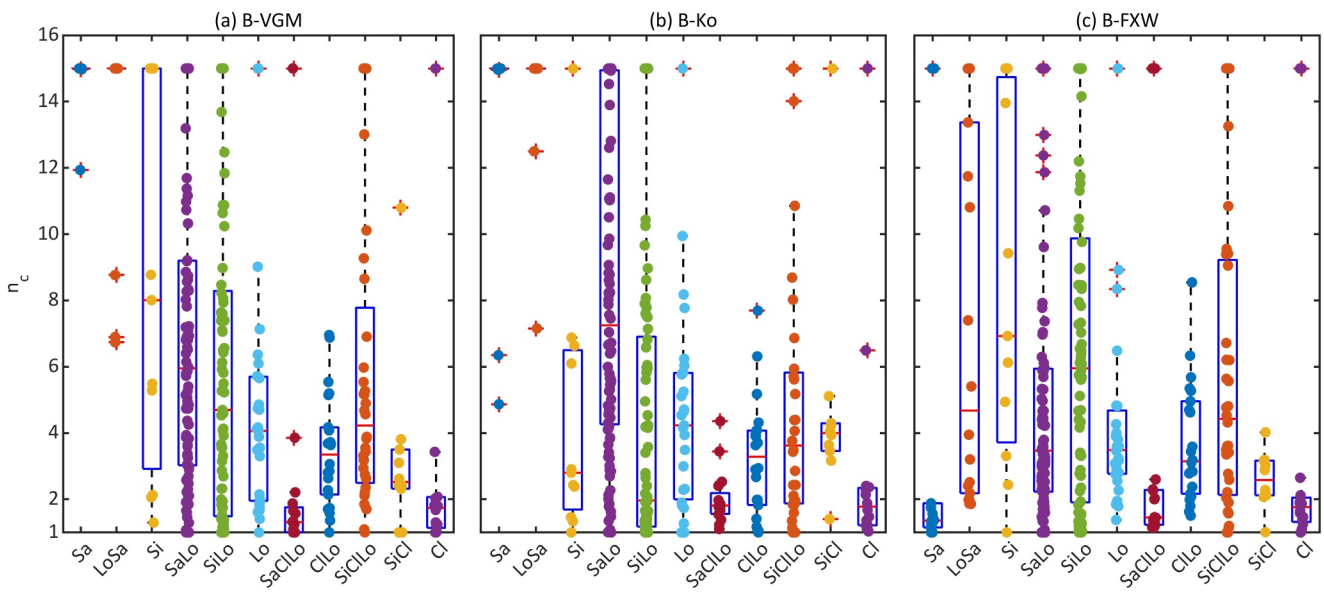

Figure 4. Distribution of n_c in different soil types for three bimodal-SWRC models. For x-lable, the soil types were sorted by increasing average clay content.

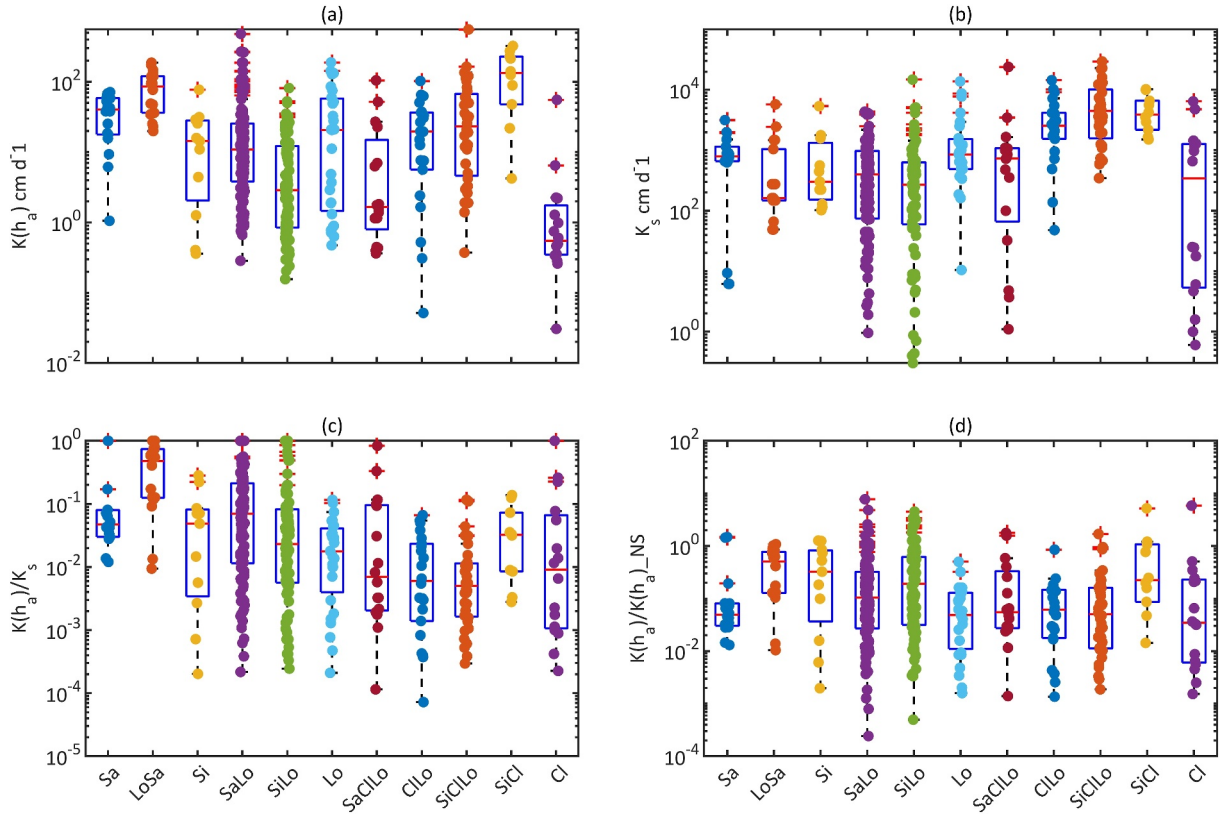

Figure 5. (a)–(d) illustrate the distribution of fitted $K(h_a)$, the measured K_S, the ratio between the fitted $K(h_a)$ and the measured K_S, and the ratio between the fitted $K(h_a)$ and the $K(h_a)\_NS$ estimated by Mualem's equation without accounting for the effects of soil structure (Equation 4) across different soil types. Here, the B-FXW model was applied for illustration.

We also directly calculated $K(h_a)$ using Mualem's model (Equation 4), denoted as $K(h_a)\_NS$. $K(h_a)\_NS$ does not account for the effects of soil structure and is widely applied in the literature. The ratio $K(h_a)/K(h_a)\_NS$ serves as an indicator of the importance of soil structure effects. The smaller the $K(h_a)/K(h_a)\_NS$, the more significant the impact of soil structure. For all soil types, the $K(h_a)/K(h_a)\_NS$ ratio is generally much smaller than 1, clearly demonstrating the effects of soil structure. The mean value of this ratio is typically between 0.01 and 0.1. The smallest ratios are mostly observed for soil types with higher clay content. Interestingly, Sand also has a very small ratio, with a median value of about 0.05. For Loamy sand and Silt, the ratio generally has a higher value, close to 1.

4.3. Prediction of Hydraulic Conductivities

4.3.1. Prediction of $K(h_a)$

Table 4 summarizes the performance of the regression method in predicting $K(h_a)$. For the training dataset, the regression method shows good performance in general. The reported *RMSE* values range from 0.45 for the U-FXW model to 0.65 for the U-VGM model, and the R^2 values range from 0.62 for the B-Ko model to 0.83 for the U-FXW model, with the U-FXW model performing the best. The model performance on the test dataset is comparable to that on the training dataset. For the test dataset, the reported *RMSE* values range from 0.43 for the U-FXW model to 0.72 for the B-Ko model, and the reported R^2 values range from 0.50 for the B-Ko model to 0.82 for the U-FXW model, with the U-FXW model again performing the best. When the B-VGM model shows a superior performance compared to the U-VGM model in predicting $K(h_a)$, the B-Ko and B-FXW models perform worse, exhibiting higher *RMSE* and lower R^2 values.

4.3.2. Prediction of Hydraulic Conductivity in Test Data Set

Figure 6 illustrates the hydraulic conductivity predictions of six proposed models evaluated with the test dataset, showing generally good agreement with observations. Among the unimodal models, the U-FXW model achieved

Table 4
Prediction of K (h_a) Using Regression Method

Model	K (h_a) (cm d^{-1})	Training		Test	
		RMSE	R^2	*RMSE*	R^2
U-VGM	$K(h_a) = 4.9461 \times 10^4(\theta_s - \theta_r)^{2.6986}\alpha^{1.0577}n^{1.9794}m^{2.0910}$	0.65	0.63	0.56	0.55
U-Ko	$K(h_a) = 1.1429 \times 10^4(\theta_s - \theta_r)^{2.8882}h_m{}^{-0.4911}\delta^{-2.0626}$	0.54	0.72	0.64	0.63
U-FXW	$K(h_a) = 1.1900 \times 10^3\theta_s{}^{1.1958}\alpha^{1.1161}n^{2.7415}m^{2.2317}$	0.45	0.83	0.43	0.82
B-VGM	$K(h_a) = 3.1354 \times 10^4(\theta_s - \theta_r)^{2.4834}\alpha^{0.8594}n^{0.1867}m^{2.5000}n_c{}^{0.6004}$	0.49	0.71	0.54	0.65
B-Ko	$K(h_a) = 5.8757 \times 10^3(\theta_s - \theta_r)^{2.7173}h_m{}^{-0.6000}\delta^{-1.2303}n_c{}^{0.4444}$	0.60	0.62	0.72	0.50
B-FXW	$K(h_a) = 4.6487 \times 10^3\theta_s{}^{1.6648}\alpha^{1.1623}n^{1.2379}m^{2.2503}n_c{}^{0.3859}$	0.49	0.65	0.49	0.63

the lowest *RMSE* of 0.465, followed by the U-VGM (0.493) and U-Ko (0.515) models. The reported R^2 is 0.769, 0.764 and 0.739 for U-FXW, U-VGM and U-Ko, respectively. The bimodal-SWRC models showed similar performance to the unimodal models in predicting HCC. The B-VGM model reported a slightly lower *RMSE* of 0.488 compared to the 0.493 of the U-VGM model. In contrast, the B-Ko and B-FXW models had slightly higher *RMSE* values of 0.556 and 0.488, respectively, compared to the 0.515 of the U-Ko model and 0.465 of the U-FXW model. The results suggest that while adding an additional parameter in bimodal models can enhance the fit (Figures 2 and 3), it may not always lead to significant improvements in predictive accuracy for all models.

4.3.3. Model Performance for Different Soil Types

Table 5 summarizes the model performance for different soil types in the test dataset, which includes 10 soil types with the number of soil samples ranging from three for Clay to 33 for Sandy loam. Overall, the proposed

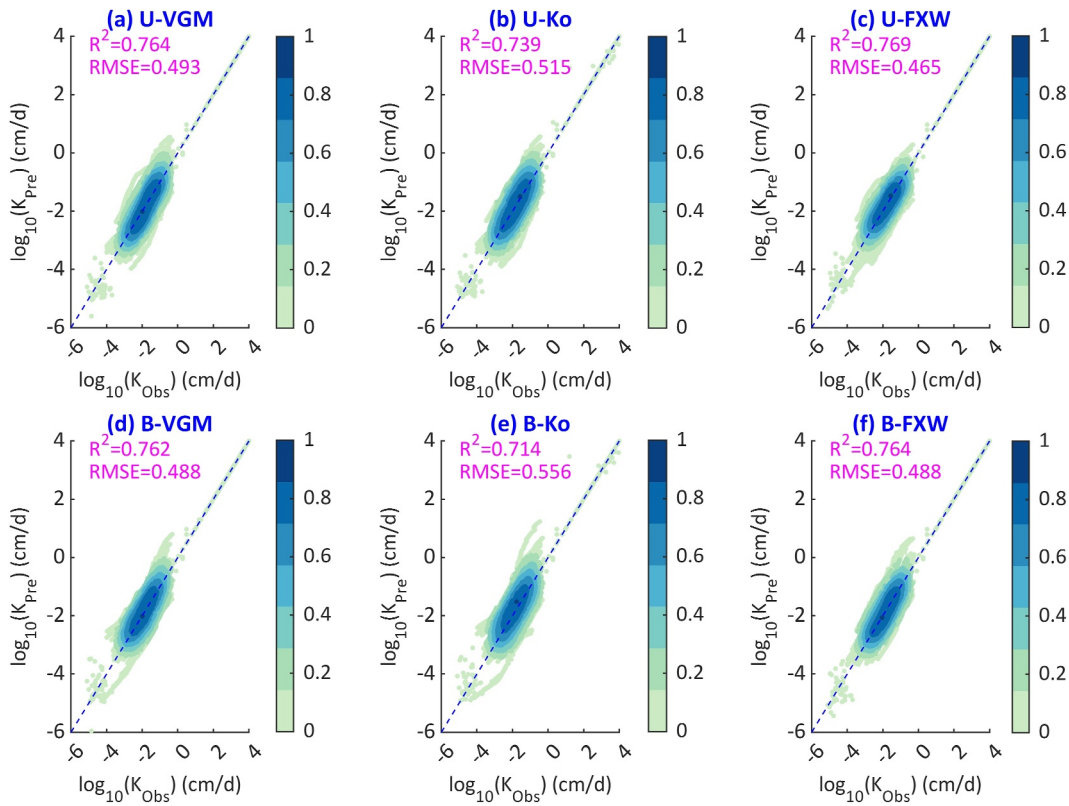

Figure 6. Prediction of hydraulic conductivity for six proposed models, testing with 107 soil samples in the test set. Panels (a) to (c) show the predicted hydraulic conductivity with three unimodal models, while panels (d) to (f) show the prediction with three bimodal models.

Table 5
Statistical Values for Ten Different Soil Types When Applying Six Models in Predicting Hydraulic Conductivity of the Test Data Set

	RMSE						R^2					
Soil type (num)	U-VGM	U-Ko	U-FXW	B-VGM	B-Ko	B-FXW	U-VGM	U-Ko	U-FXW	B-VGM	B-Ko	B-FXW
'Cl' (3)	0.60	0.62	0.60	**0.51**	0.58	0.53	0.81	**0.87**	0.76	0.80	0.85	0.79
'ClLo' (10)	0.64	0.61	0.62	**0.41**	0.65	0.54	0.71	0.65	0.72	**0.85**	0.72	0.77
'Lo' (10)	0.48	0.54	**0.46**	0.55	0.59	0.54	**0.79**	0.74	0.77	0.76	0.72	0.76
'LoSa' (4)	0.84	0.89	0.75	0.53	0.65	**0.47**	0.84	0.83	**0.92**	0.85	0.79	**0.92**
'Sa' (6)	0.47	0.52	0.56	0.78	0.93	**0.43**	0.89	0.87	**0.90**	0.70	0.61	**0.90**
'SaClLo' (3)	**0.50**	0.59	0.55	**0.50**	0.59	0.54	**0.69**	0.60	0.63	0.67	0.60	0.62
'SaLo' (33)	0.43	0.50	**0.39**	0.43	0.51	0.41	0.82	0.78	0.83	**0.84**	0.79	**0.84**
'SiCl' (3)	0.29	0.36	**0.27**	0.44	0.46	0.43	0.97	0.96	0.96	0.87	0.90	**0.98**
'SiClLo' (10)	0.58	**0.51**	0.55	0.55	0.60	0.59	0.75	**0.79**	0.76	0.74	0.72	0.71
'SiLo' (25)	0.43	0.42	**0.39**	0.48	0.48	0.49	0.77	0.76	**0.79**	0.72	0.71	0.71
Mean	0.53	0.56	0.51	0.52	0.60	**0.50**	0.80	0.79	0.80	0.78	0.74	0.80

framework performed well in predicting hydraulic conductivities, with all six models generally reporting *RMSE* values below 0.60 and R^2 values higher than 0.70. However, the performance in different soil types varied among the different models. Among the six models, the U-FXW model achieved the lowest *RMSE* values for four soil types (Loam, Sandy loam, Silty clay and Silty loam), followed by the B-VGM model for three soil types (Clay, Clay loam and Sandy clay loam), and the B-FXW model for two soil types (Loamy sand and Sand). Both the U-Ko and B-Ko models showed relatively higher *RMSE* values for most soil types, making them less recommended.

A comparison between bimodal-SWRC and unimodal-SWRC models indicates that bimodal-SWRC models do not consistently offer a significant improvement in predicting HCC for all soil types. Notably, the HCC of the unimodal-SWRC models is also capable of capturing the effects of soil structure.

4.4. Evaluation With Independent Soil Samples

Figure 7 illustrates the model performance using 52 soil samples from the UNSODA dataset. The proposed framework performed exceptionally well in describing SHPs across the entire moisture range. The three unimodal-SWRC models closely matched the observed SWRC, showing no significant overestimation in the dry range, as previously noted in dataset from Hohenbrink et al. (2023) (Figure 2). The R^2 values were all above 0.99, and the *RMSE* was approximately 0.012 $cm^3\ cm^{-3}$ for all three unimodal-SWRC models. The empirically based regression method effectively predicted K (h_a), ensuring an overall accurate estimation of HCC with the unimodal-SWRC models. The *RMSE* was about 0.67 for both the U-VGM and U-FXW models, and 0.70 for the U-Ko model.

Compared to the unimodal-SWRC models, the three bimodal-SWRC models improved the fitting of SWRC, reducing the *RMSE* to about 0.010 $cm^3\ cm^{-3}$. For the selected UNSODA dataset, several soil samples clearly exhibited bimodal-shaped SWRCs, as highlighted by Wang et al. (2023). The considerable improvement in fitting SWRCs suggested the proposed bimodal-SWRC models can well capture the bimodal shape SWRCs. In terms of HCC, the bimodal-SWRC models slightly increased the R^2 values while maintaining similar *RMSE* values.

Overall, when considering both SWRC fitting and HCC prediction, the B-FXW model performed the best among the tested models.

Figures 8 and 9 present the predictions of hydraulic conductivity for 10 soil samples from other data sources using unimodal and bimodal models, respectively. The three unimodal models generally showed good agreement with observations. However, they failed to capture the bimodal shape of the SWRC in four out of the 10 soil samples.

In terms of hydraulic conductivity prediction, the three unimodal models were generally in good agreement with observations for almost all 10 soil samples. However, for the four soil samples that exhibit bimodal SWRC (Figures 8d–8g and 8i), the three unimodal models underestimated K (h_a) and then underestimated the hydraulic

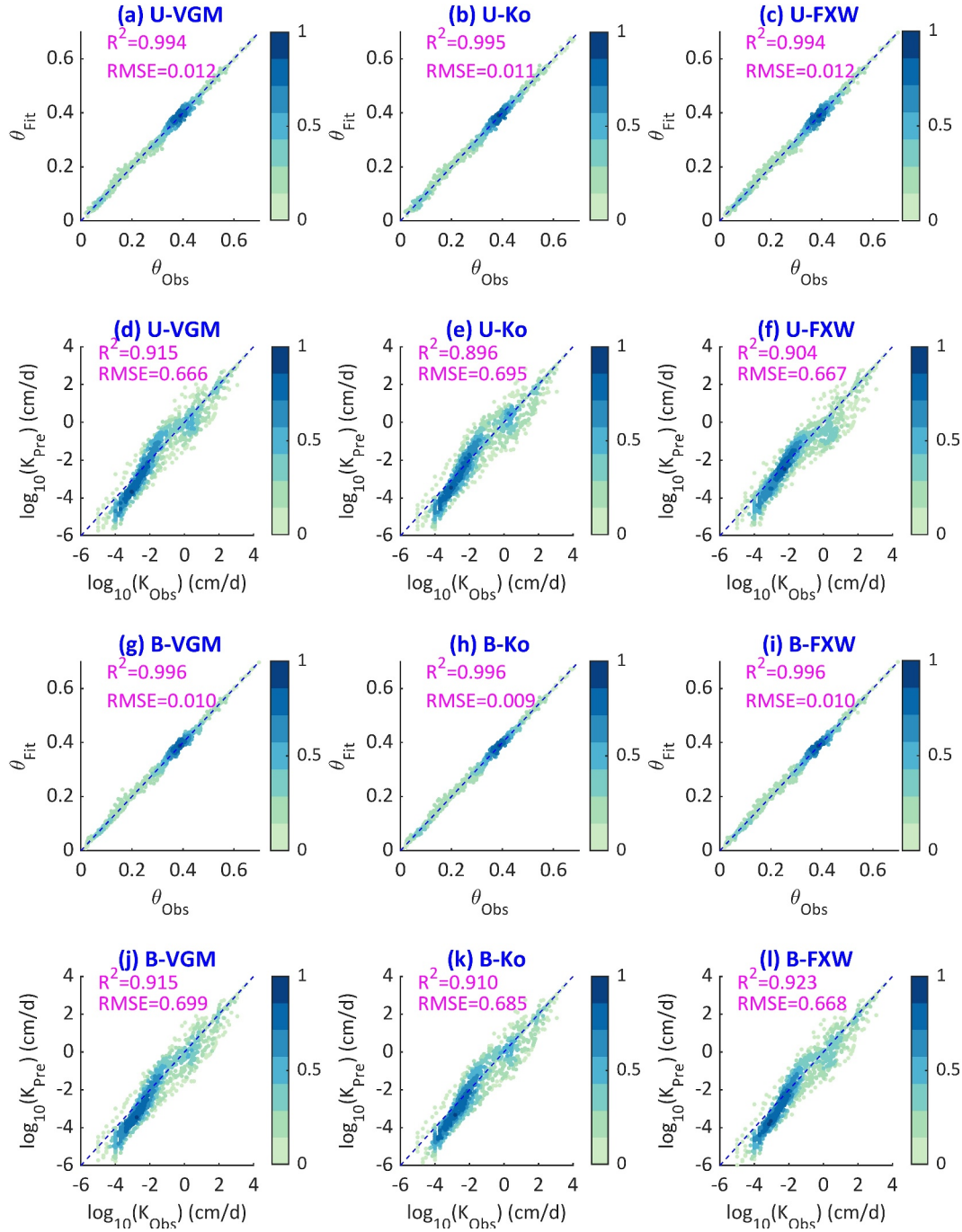

Figure 7. Performance of six proposed models in fitting soil water retention curve (SWRC) and predicting hydraulic conductivity curve (HCC) when evaluated with 52 independent soil samples from the unsaturated soil hydraulic database dataset. Panels (a) to (f) show the fitted SWRC and predicted HCC with three unimodal models, while panels (g) to (i) show the fitted SWRC and predicted HCC with three bimodal models.

conductivity. Although the three unimodal models could not capture the bimodal shape of the SWRC, they could capture the bimodal HCC by introducing an additional parameter of K (h_a), as shown in one silt loam soil sample (Figure 8f) and one clay sample (Figure 8i).

The three bimodal models, as shown in Figure 9, achieved better performance in fitting the bimodal SWRC compared to the unimodal models. With one additional free-fitted parameter n_c, they effectively captured the

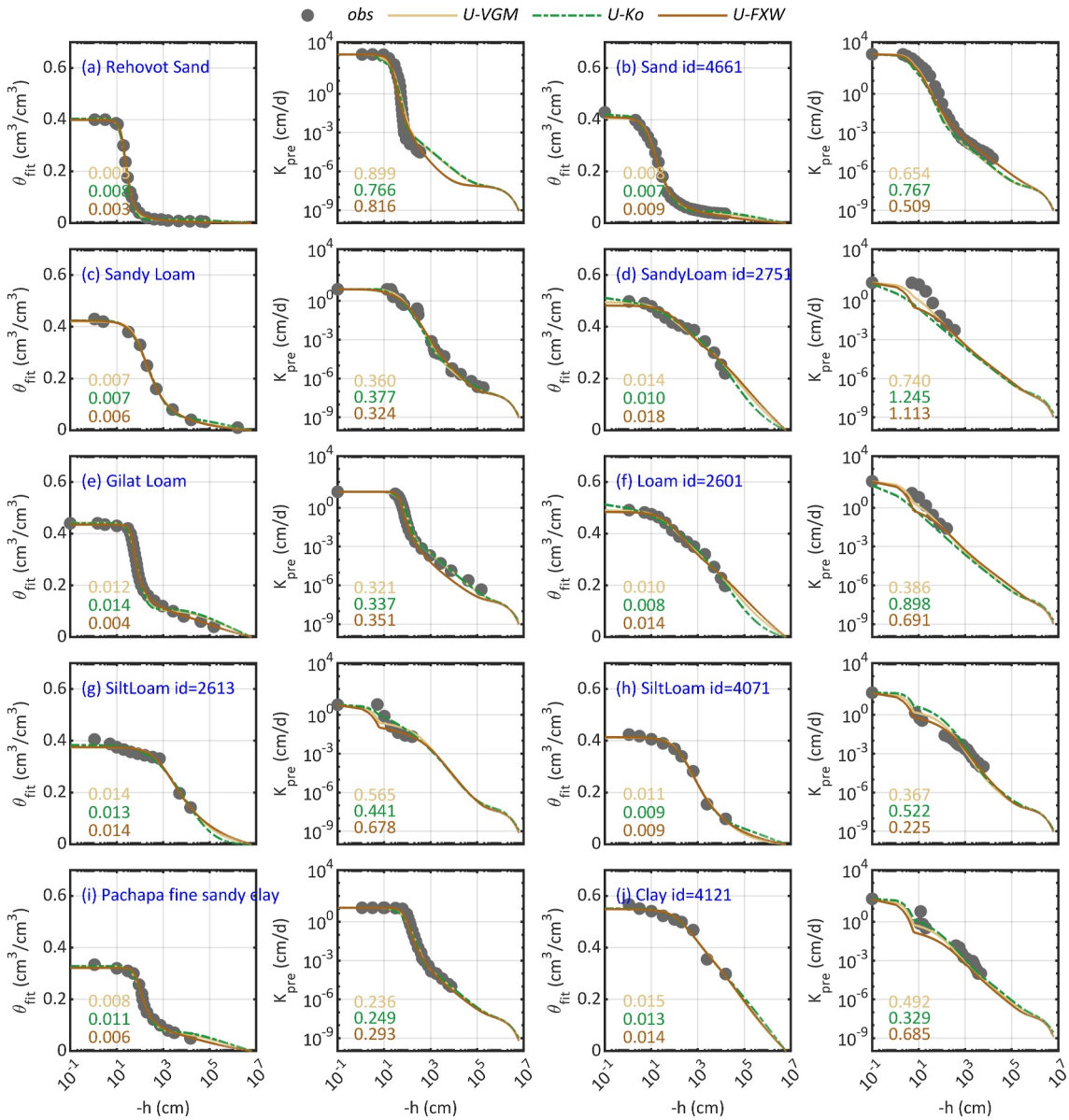

Figure 8. Model performance of three unimodal models, testing with 10 soil samples from literature. Rohovot sand (a), Gilat loam (e) and Pachapa fine sandy clay (f) come from Mualem (1976b); The other six soil samples come from the unsaturated soil hydraulic database (Nemes et al., 2001).

bimodal shape of the SWRC. For the six soil samples exhibiting unimodal SWRC, the three bimodal models performed very well in predicting HCC, comparable to the performance of the three unimodal models. For the four soil samples with bimodal SWRC, the three bimodal models significantly improved the prediction of HCC compared to the three unimodal models. However, an exception was noted with the B-Ko model, which showed poorer performance for one silt loam soil sample compared to the U-Ko model (Figure 9g).

5. Discussion

5.1. Widespread Effects of Soil Structure

We applied the ratio $K(h_a)/K(h_a)$_NS to represent the effects of soil structure, particularly macropores. For most of the 355 soil samples, there is a clear effect of soil structure, as identified by a general $K(h_a)/K(h_a)$_NS value between 0.01 and 0.1 (Figure 5d). This effect is observed across all 10 soil types, with smaller ratios mostly noted for soil types with higher clay content and higher ratios for Sandy loam and Silt. Interestingly, Sand also shows a

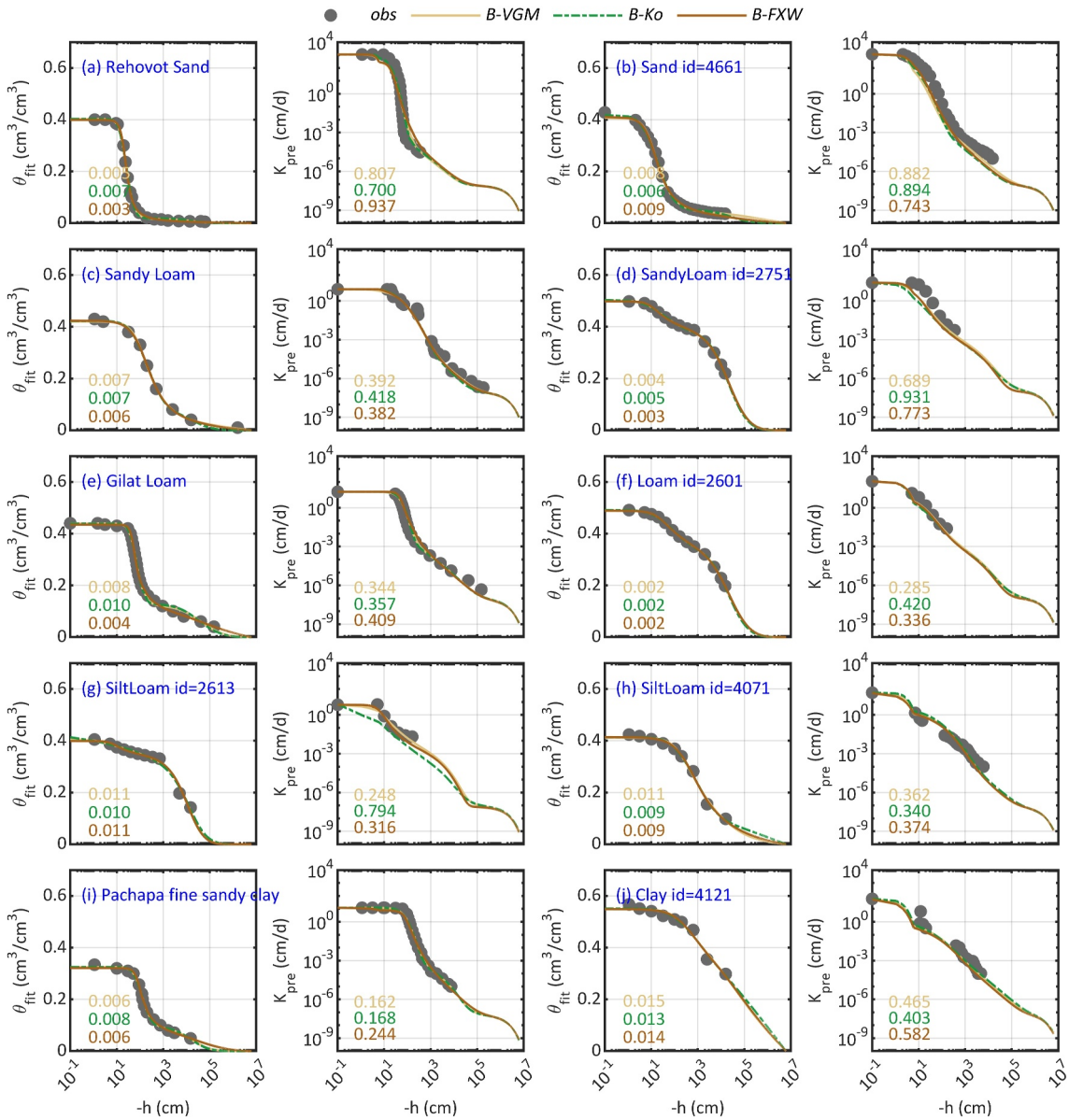

Figure 9. Model performance of three bimodal models, testing with 10 soil samples from literature. Rohovot sand (a), Gilat loam (e) and Pachapa fine sandy clay (f) come from Mualem (1976b); The other six soil samples come from the unsaturated soil hydraulic database (Nemes et al., 2001).

very small ratio, with a median value of about 0.05. These results suggest that the effects of soil structure (macropores) are widespread not only in fine-textured soils but also in coarse-textured soils, consistent with the findings of Zhang et al. (2022).

The effects of soil structure resulting from a bimodal distribution of pore sizes are also noticed for most samples. As shown, the bimodal-SWRC models have a superior performance over unimodal-SWRC models for most soil samples, as indicated by lower AIC values (Table 3). These results confirm the widespread effects of soil structure due to a bimodal distribution of pore sizes. Although the bimodal SWRC models only slightly improved the prediction of HCC compared to unimodal SWRC models, it should be noted that the slope of the SWRC and thus the soil flux could differ significantly between the two models. Further investigation is needed to understand the effects on soil water hydrology processes resulting from the application of unimodal and bimodal models.

Given the widespread effects of soil structure, it is important to use SHMs that account for these effects in vadose zone hydrology. However, currently, the unimodal SHM remains the mainstream approach applied in soil hydrology-related processes (e.g., Fatichi et al., 2020; Vereecken et al., 2022; Zhang et al., 2022).

5.2. Model Comparison

This study presents a generalized framework to describe both unimodal and bimodal SHPs across the entire saturation range. This framework incorporates the effects of soil structure, capillarity, adsorption forces, and vapor diffusion. The key innovation is the introduction of a scaling factor to scale the capillarity-associated SWRC, introducing one parameter n_c. It also includes a saturated matrix hydraulic conductivity, $K(h_a)$, to account for the effects of soil structure on the HCC. $K(h_a)$ is further estimated from the parameters of SWRC. This framework can be easily applied with any SHM that accounts for capillary forces. Here, we applied VG model, Kosugi model and FX model for describing the SWRC associated with capillary forces.

When n_c is set to a constant of 1, the unimodal model can capture the bimodal HCC but is not flexible enough to capture the bimodal SWRC. This unimodal model is well-suited for situations where small changes in water content near saturation are no longer detectable via measured SWRC, yet soil structure still causes a sharp decline in HCC near saturation. When n_c is treated as a free-fitted parameter, the bimodal model can capture both bimodal SWRC and HCC. This bimodal model is well-suited for situations where bimodal SWRC is clearly shown due to a bimodal particle size distribution (Turturro et al., 2022). An examination of n_c distribution suggested no clear pattern or relationship between n_c and soil properties. Since n_c and the other four parameters collectively determine the SWRC, it is more appropriate to interpret n_c simply as a shaping factor.

The proposed three unimodal models have four free-fitted parameters, the same as the widely used VGM model. Unlike the VGM model, which only considers capillary forces, the proposed models account for additional effects of soil structure on HCC and adsorption forces on both SWRC and HCC. The evaluation dataset shows that the proposed models are in good agreement with observations over the entire saturation range. In contrast, the VGM model is known to overestimate HCC in the wet range and underestimate it in the dry range (e.g., Schaap & Van Genuchten, 2006; Wang et al., 2023).

In the past two decades, many SHMs have been developed to account for both capillary and adsorption forces. Although these models claim to describe SHPs across the full moisture range, they often neglect the effects of soil structure, leading to an overall overestimation of hydraulic conductivity (e.g., Liao et al., 2018; Stanić et al., 2020; Wang et al., 2016; Weber et al., 2019; Yang et al., 2023).

Wang et al. (2023) recently developed a new hydraulic conductivity model that considers the effects of soil structure, capillarity, and adsorption forces. The FXW-M3 model developed by Wang et al. (2023) is very similar to the U-FXW model proposed in this study. The difference lies in how $K(h_a)$ is estimated: Wang et al. (2023) use a physical method developed by Wang, Ma, and Zhu (2022), while the U-FXW model uses a regression approach. Evaluation with the same 52 soil samples from the UNSODA dataset suggested that the U-FXW model has superior performance compared to the FXW-M3 model, with reported *RMSE* values of 0.67 and 0.78 (Wang et al., 2023) and R^2 values of 0.90 and 0.88 (Wang et al., 2023), respectively. As discussed in Wang et al. (2023), the FXW-M3 model exhibited some obvious underestimation of hydraulic conductivity for certain soil samples due to the uncertainty in estimating $K(h_a)$. In contrast, the regression method developed here performed better in predicting $K(h_a)$. One shortcoming of both the FXW-M3 and U-FXW models is that K_c was derived empirically based on the method by Wang et al. (2018). This study improves on this by using the van Genuchten (1980) model and Kosugi (1994) model to describe the SWRC associated with capillary forces, leading to a closed-form K_c function derived using Mualem (1976a)'s model.

Another recent example addressing the combined effects of soil structure, capillarity, adsorption forces, and vapor diffusion is the updated PDI model (Iden & Durner, 2014; Peters, 2013), as proposed by Peters et al. (2023). The updated PDI model differs from the FXW-M3 model (Wang et al., 2023) and the three unimodal models in this study in three key aspects.

1. **Construction of the SWRC function**: In Wang et al. (2023) and this study, the scaling function $C(h)$ is multiplied by the total water content, resulting in a mathematically continuous SWRC function across the entire moisture range. In contrast, the PDI model superimposes capillary and non-capillary water retention,

with both components reaching zero water content at complete dryness. The PDI model also requires an additional smoothing method (Iden & Durner, 2014) to achieve a mathematically continuous SWRC function.

2. **Description of K_f**: In the FXW-M3 model and the U-FXW model, adsorption forces are empirically incorporated into the hydraulic conductivity function, requiring no additional expression (Equation A2). Although the expression differs slightly in the PDI model and the U-VGM and U-Ko models proposed here, they all derive from Tokunaga (2009) model. Additionally, all models estimate film conductivity directly from the SWRC, inspired by the original work of Lebeau and Konrad (2010). Following Lebeau and Konrad (2010), the U-VGM and U-Ko models proposed here account for ionic-electrostatic interactions and molecular components, as well as increased viscosity near mineral surfaces when the film thickness is less than 10 nm. In contrast, the PDI model neglects these molecular components and viscosity increases. While the approach in the Lebeau and Konrad (2010) is more physically grounded, Peters et al. (2021) found minimal performance differences between the methods.
3. **Prediction of $K(h_a)$**: The FXW-M3 model (Wang et al., 2023) uses the estimated hydraulic conductivity in the matric potential of h_m as a matching point to estimate $K(h_a)$. The three unimodal models developed here employ a regression method to estimate $K(h_a)$ from the SWRC parameters. In contrast, the updated PDI model introduces an empirically derived saturated tortuosity parameter to estimate $K(h_a)$.

However, the models developed in Wang et al. (2023) and in Peters et al. (2023) cannot capture bimodal SWRC, while the model proposed here can capture bimodal SWRC in the cost of introducing one additional free-fitted parameter.

With a total of five free-fitted parameters, the proposed bimodal framework can capture both bimodal SWRC and HCC. In contrast, widely used bimodal models in the literature, such as the bimodal VGM model developed by Durner (1994), generally require six to seven free-fitted parameters. Thus, the proposed framework significantly reduces model complexity, providing a practical tool for field applications. Additionally, the developed bimodal models account for adsorption forces, which are not considered in commonly used bimodal models. When the proposed three bimodal models all performed well in describing SHPs, the B-FXW model performed the best for most soil samples. Notably, when needed, h_r can also be treated as a free-fitted parameter to increase the flexibility of the proposed models in describing bimodal SWRCs; however, this approach may increase the uncertainty in predicting HCCs.

5.3. Model Limitations

While the proposed models perform well in describing SHPs across the entire moisture range, they do have some limitations.

One limitation is the uncertainty in estimating $K(h_a)$ from the parameters of the fitted SWRC. The fitted $K(h_a)$ is generally in the range from 1 to 100 cm d^{-1} (Figure 5). However, $K(h_a)$ does show considerable variability even within the same soil type. As shown with the evaluation dataset, the estimated $K(h_a)$ deviates from the optimized value, resulting in *RMSE* values of HCC prediction that are approximately twice those of the optimized value. Meanwhile, the regression method for predicting $K(h_a)$ from SWRC is essentially empirical and lacks a physical basis.

Another limitation pertains to the bimodal models. The K_c of the proposed bimodal models must be derived numerically, which partially increases the model's complexity. In contrast, the closed-form hydraulic conductivity functions of commonly applied bimodal models can be found in the literature. However, compared to these commonly used bimodal models, the new models significantly reduce the number of free-fitted parameters, enhancing their practicality.

6. Conclusions

Soil hydraulic properties are influenced by complex factors such as soil structure, capillarity, and adsorption forces, exhibiting different characteristics across varying moisture levels and often presenting bimodal features. Traditional SHMs rarely consider all these interacting forces, or they require the introduction of more parameters to capture these characteristics, increasing model complexity and reducing practical applicability.

This study presents a generalized framework to describe unimodal and bimodal SHPs over the entire saturation degree range. The framework can be applied with any SHM that accounts for capillary forces. The framework

accounts for the effects of soil structure, capillarity, adsorption forces, and vapor diffusion. By employing a regression method, we establish a relationship between the introduced saturated matrix hydraulic conductivity $K(h_a)$ and the parameters of the SWRC, further reducing the number of the free-fitted parameters. Meanwhile, the SWRC of the proposed framework is mathematically continuous over the entire moisture range, facilitating its application in numerical modeling.

In its form with four free-fitted parameters, equivalent to the widely applied capillarity-based models, the proposed framework can capture the bimodal HCC but is not flexible enough to capture bimodal SWRC. In its form with five free-fitted parameters, the proposed model can capture both bimodal SWRC and bimodal HCC.

Validation using 355 soil samples from a recent soil database and 52 independent soil samples from UNSODA dataset demonstrates that the new framework effectively represents SHPs across the full moisture range, accurately capturing the influences of soil structure, capillarity, adsorption forces, and vapor diffusion. Among the six proposed models, the bimodal B-FXW model has a superior performance, indicated by a low AIC value for most samples. Given its ability to characterize SHPs over the entire moisture range without significantly increasing model complexity, the new model holds considerable promise for practical applications.

Appendix A: The HCC of the U-FXW Model

The HCC of the U-FXW model is given as

$$K = K_l + K_v \tag{A1}$$

where K_l is the hydraulic conductivity of liquid soil water, accounting for the effects of capillary and adsorption forces. K_l can be described by the HCC of the FXW-M3 model (Wang et al., 2023), which is expressed as

$$K_l(h) = \begin{cases} K(h_a)\left(\dfrac{\Gamma(h)-\Gamma(h_0)}{\Gamma(h_a)-\Gamma(h_0)}\right)^{l}\left[\dfrac{1-\left(1-\Gamma(h)^{1/m}\right)^{1-1/n}}{1-\left(1-\Gamma(h_a)^{1/m}\right)^{1-1/n}}\right]^2 & h < h_a \\ K_s\Gamma(h)^{\frac{\ln(K(h_a)/K_s)}{\ln(\Gamma(h_a))}} & h \geq h_a \end{cases} \tag{A2}$$

where l equals 3.5 as suggested by Wang et al. (2018).

Data Availability Statement

The applied data from UNSODA can be accessed at the website of the United States Department of Agriculture (https://data.nal.usda.gov/dataset/unsoda-20-unsaturated-soil-hydraulic-database-database-and-program-indirect-methods-estimating-unsaturated-hydraulic-properties). The applied data is also provided in Data Set S1. The applied data from Hohenbrink et al. (2023) can be accessed via https://doi.org/10.5880/fidgeo.2023.012.

Acknowledgments
This research was supported in part by the National Natural Science Foundation of China (Grant 42071045; U2244230; 42425207) and in part by Natural Science Foundation of Hubei (2024AFD376). The authors acknowledge the anonymous reviewers and Wolfgang Durner for their insightful comments that improved the manuscript.

References

Akaike, H. (1974). A new look at the statistical model identification. *IEEE Transactions on Automatic Control*, *19*(6), 716–723. https://doi.org/10.1109/tac.1974.1100705

Børgesen, C. D., Jacobsen, O. H., Hansen, S., & Schaap, M. G. (2006). Soil hydraulic properties near saturation, an improved conductivity model. *Journal of Hydrology*, *324*(1–4), 40–50. https://doi.org/10.1016/j.jhydrol.2005.09.014

Campbell, G. S., & Shiozawa, S. (1992). Prediction of hydraulic properties of soils using particle-size distribution and bulk density data. In M.Th. vanGenuchten, F. J. Leij, & L. J. Lund (Eds.), *Proceedings of the international workshop on indirect methods for estimating the hydraulic properties of unsaturated soil* (pp. 317–328). University of California.

Childs, E. C., & Collis-George, N. (1950). The permeability of porous materials. *Proceedings of the Royal Society of London - Series A: Mathematical and Physical Sciences*, *201*(1066), 392–405.

Clark, M. P., Fan, Y., Lawrence, D. M., Adam, J. C., Bolster, D., Gochis, D. J., et al. (2015). Improving the representation of hydrologic processes in earth system models. *Water Resources Research*, *51*(8), 5929–5956. https://doi.org/10.1002/2015wr017096

de Rooij, G. H. (2024). Averaging or adding domain conductivities to calculate the unsaturated soil hydraulic conductivity. *Vadose Zone Journal*, e20329.

de Rooij, G. H., Mai, J., & Madi, R. (2021). Sigmoidal water retention function with improved behaviour in dry and wet soils. *Hydrology and Earth System Sciences*, *25*(2), 983–1007. https://doi.org/10.5194/hess-25-983-2021

Diamantopoulos, E., & Durner, W. (2013). Physically-based model of soil hydraulic properties accounting for variable contact angle and its effect on hysteresis. *Advances in Water Resources*, *59*, 169–180. https://doi.org/10.1016/j.advwatres.2013.06.005
Du, C. (2020). Comparison of the performance of 22 models describing soil water retention curves from saturation to oven dryness. *Vadose Zone Journal*, *19*(1), e20072. https://doi.org/10.1002/vzj2.20072
Duan, Q., Sorooshian, S., & Gupta, V. (1992). Effective and efficient global optimization for conceptual rainfall-runoff models. *Water Resources Research*, *28*(4), 1015–1031. https://doi.org/10.1029/91wr02985
Durner, W. (1994). Hydraulic conductivity estimation for soils with heterogeneous pore structure. *Water Resources Research*, *30*(2), 211–223. https://doi.org/10.1029/93wr02676
Fatichi, S., Or, D., Walko, R., Vereecken, H., Young, M. H., Ghezzehei, T. A., et al. (2020). Soil structure is an important omission in Earth System Models. *Nature Communications*, *11*(1), 522. https://doi.org/10.1038/s41467-020-14411-z
Fayer, M. J., & Simmons, C. S. (1995). Modified soil water retention functions for all matric suctions. *Water Resources Research*, *31*(5), 1233–1238. https://doi.org/10.1029/95wr00173
Fredlund, D. G., & Xing, A. (1994). Equations for the soil-water characteristic curve. *Canadian Geotechnical Journal*, *31*(4), 521–532. https://doi.org/10.1139/t94-061
Gerke, H. H. (2006). Preferential flow descriptions for structured soils. *Journal of Plant Nutrition and Soil Science*, *169*(3), 382–400. https://doi.org/10.1002/jpln.200521955
Gutmann, E. D., & Small, E. E. (2007). A comparison of land surface model soil hydraulic properties estimated by inverse modeling and pedotransfer functions. *Water Resources Research*, *43*(5). https://doi.org/10.1029/2006wr005135
Hohenbrink, T. L., Jackisch, C., Durner, W., Germer, K., Iden, S. C., Kreiselmeier, J., et al. (2023). Soil water retention and hydraulic conductivity measured in a wide saturation range. *Earth System Science Data*, *15*(10), 4417–4432. https://doi.org/10.5194/essd-15-4417-2023
Iden, S. C., & Durner, W. (2014). Comment on'Simple consistent models for water retention and hydraulic conductivity in the complete moisture range'by A. Peters. *Water Resources Research*, *50*(9), 7530–7534. https://doi.org/10.1002/2014wr015937
Jarvis, N. J. (2007). A review of non-equilibrium water flow and solute transport in soil macropores: Principles, controlling factors and consequences for water quality. *European Journal of Soil Science*, *58*(3), 523–546. https://doi.org/10.1111/j.1365-2389.2007.00915.x
Jarvis, N. J., Jansson, P. E., Dik, P. E., & Messing, I. (1991). Modelling water and solute transport in macroporous soil. I. Model description and sensitivity analysis. *Journal of Soil Science*, *42*(1), 59–70. https://doi.org/10.1111/j.1365-2389.1991.tb00091.x
Khlosi, M., Cornelis, W. M., Gabriels, D., & Sin, G. (2006). Simple modification to describe the soil water retention curve between saturation and oven dryness. *Water Resources Research*, *42*(11). https://doi.org/10.1029/2005wr004699
Kosugi, K. I. (1994). Three-parameter lognormal distribution model for soil water retention. *Water Resources Research*, *30*(4), 891–901. https://doi.org/10.1029/93wr02931
Kosugi, K. I. (1996). Lognormal distribution model for unsaturated soil hydraulic properties. *Water Resources Research*, *32*(9), 2697–2703. https://doi.org/10.1029/96wr01776
Larsbo, M., Roulier, S., Stenemo, F., Kasteel, R., & Jarvis, N. (2005). An improved dual-permeability model of water flow and solute transport in the vadose zone. *Vadose Zone Journal*, *4*(2), 398–406. https://doi.org/10.2136/vzj2004.0137
Lebeau, M., & Konrad, J.-M. (2010). A new capillary and thin film flow model for predicting the hydraulic conductivity of unsaturated porous media. *Water Resources Research*, *46*(12), W12554. https://doi.org/10.1029/2010WR009092
Liao, K., Lai, X., Zhou, Z., Zhu, Q., & Han, Q. (2018). A simple and improved model for describing soil hydraulic properties from saturation to oven dryness. *Vadose Zone Journal*, *17*(1), 1–8. https://doi.org/10.2136/vzj2018.04.0082
Lu, S., Ren, T., Gong, Y., & Horton, R. (2008). Evaluation of three models that describe soil water retention curves from saturation to oven dryness. *Soil Science Society of America Journal*, *72*(6), 1542–1546. https://doi.org/10.2136/sssaj2007.0307n
Madejón, P., Domínguez, M. T., Fernández-Boy, E., Paneque, P., Girón, I., & Madejón, E. (2019). Soil hydraulic properties as the main driver in the establishment of biomass crops in contaminated soils. *Journal of Environmental Management*, *233*, 812–822. https://doi.org/10.1016/j.jenvman.2018.10.008
Millington, R. J., & Quirk, J. P. (1961). Permeability of porous solids. *Transactions of the Faraday Society*, *57*, 1200–1207. https://doi.org/10.1039/tf9615701200
Morel-Seytoux, H. J., & Nimmo, J. R. (1999). Soil water retention and maximum capillary drive from saturation to oven dryness. *Water Resources Research*, *35*(7), 2031–2041. https://doi.org/10.1029/1999wr900121
Mualem, Y. (1976a). A new model for predicting the hydraulic conductivity of unsaturated porous media. *Water Resources Research*, *12*(3), 513–522. https://doi.org/10.1029/wr012i003p00513
Mualem, Y. (1976b). A catalogue of the hydraulic properties of unsaturated soils. *Technical Report, Israel Institute of Technology*, 28–70.
Nemes, A. D., Schaap, M. G., Leij, F. J., & Wösten, J. H. M. (2001). Description of the unsaturated soil hydraulic database UNSODA version 2.0. *Journal of Hydrology*, *251*(3–4), 151–162. https://doi.org/10.1016/s0022-1694(01)00465-6
Nimmo, J. R. (1991). Comment on the treatment of residual water content in "A consistent set of parametric models for the two-phase flow of immiscible fluids in the subsurface" by L. Luckner et al. *Water Resources Research*, *27*(4), 661–662. https://doi.org/10.1029/91wr00165
Othmer, H., Diekkrüger, B., & Kutilek, M. (1991). Bimodal porosity and unsaturated hydraulic conductivity. *Soil Science*, *152*(3), 139–150. https://doi.org/10.1097/00010694-199109000-00001
Peters, A. (2013). Simple consistent models for water retention and hydraulic conductivity in the complete moisture range. *Water Resources Research*, *49*(10), 6765–6780. https://doi.org/10.1002/wrcr.20548
Peters, A., Hohenbrink, T. L., Iden, S. C., & Durner, W. (2021). A simple model to predict hydraulic conductivity in medium to dry soil from the water retention curve. *Water Resources Research*, *57*(5), e2020WR029211. https://doi.org/10.1029/2020wr029211
Peters, A., Hohenbrink, T. L., Iden, S. C., van Genuchten, M. T., & Durner, W. (2023). Prediction of the absolute hydraulic conductivity function from soil water retention data. *Hydrology and Earth System Sciences*, *27*(7), 1565–1582. https://doi.org/10.5194/hess-27-1565-2023
Pinheiro, E. A. R., van Lier, Q. D. J., & Šimůnek, J. (2019). The role of soil hydraulic properties in crop water use efficiency: A process-based analysis for some Brazilian scenarios. *Agricultural Systems*, *173*, 364–377. https://doi.org/10.1016/j.agsy.2019.03.019
Romano, N., Nasta, P., Severino, G., & Hopmans, J. W. (2011). Using bimodal lognormal functions to describe soil hydraulic properties. *Soil Science Society of America Journal*, *75*(2), 468–480. https://doi.org/10.2136/sssaj2010.0084
Ross, P. J., & Smettem, K. R. (1993). Describing soil hydraulic properties with sums of simple functions. *Soil Science Society of America Journal*, *57*(1), 26–29. https://doi.org/10.2136/sssaj1993.03615995005700010006x
Rossi, C., & Nimmo, J. R. (1994). Modeling of soil water retention from saturation to oven dryness. *Water Resources Research*, *30*(3), 701–708. https://doi.org/10.1029/93wr03238
Saito, H., Šimůnek, J., & Mohanty, B. P. (2006). Numerical analysis of coupled water, vapor, and heat transport in the vadose zone. *Vadose Zone Journal*, *5*(2), 784–800. https://doi.org/10.2136/vzj2006.0007

Schaap, M. G., & Leij, F. J. (2000). Improved prediction of unsaturated hydraulic conductivity with the Mualem-van Genuchten model. *Soil Science Society of America Journal*, *64*(3), 843–851. https://doi.org/10.2136/sssaj2000.643843x

Schaap, M. G., Leij, F. J., & Van Genuchten, M. T. (2001). Rosetta: A computer program for estimating soil hydraulic parameters with hierarchical pedotransfer functions. *Journal of Hydrology*, *251*(3–4), 163–176. https://doi.org/10.1016/s0022-1694(01)00466-8

Schaap, M. G., & Van Genuchten, M. T. (2006). A modified Mualem–van Genuchten formulation for improved description of the hydraulic conductivity near saturation. *Vadose Zone Journal*, *5*(1), 27–34. https://doi.org/10.2136/vzj2005.0005

Schneider, M., & Goss, K. U. (2012). Prediction of the water sorption isotherm in air dry soils. *Geoderma*, *170*, 64–69. https://doi.org/10.1016/j.geoderma.2011.10.008

Seneviratne, S. I., Corti, T., Davin, E. L., Hirschi, M., Jaeger, E. B., Lehner, I., et al. (2010). Investigating soil moisture–climate interactions in a changing climate: A review. *Earth-Science Reviews*, *99*(3–4), 125–161. https://doi.org/10.1016/j.earscirev.2010.02.004

Šimůnek, J., & van Genuchten, M. T. (2008). Modeling nonequilibrium flow and transport processes using HYDRUS. *Vadose Zone Journal*, *7*(2), 782–797.

Šimůnek, J., Van Genuchten, M. T., & Šejna, M. (2016). Recent developments and applications of the HYDRUS computer software packages. *Vadose Zone Journal*, *15*(7), 1–25. vzj2016-04. https://doi.org/10.2136/vzj2016.04.0033

Stanić, F., Delage, P., Tchiguirinskaia, I., Versini, P. A., Cui, Y. J., & Schertzer, D. (2020). A new fractal approach to account for capillary and adsorption phenomena in the water retention and transfer properties of unsaturated soils. *Water Resources Research*, *56*(12), e2020WR027808. https://doi.org/10.1029/2020wr027808

Tokunaga, T. K. (2009). Hydraulic properties of adsorbed water films in unsaturated porous media. *Water Resources Research*, *45*(6), W06415. https://doi.org/10.1029/2009wr007734

Tuller, M., & Or, D. (2001). Hydraulic conductivity of variably saturated porous media: Film and corner flow in angular pore space. *Water Resources Research*, *37*(5), 1257–1276. https://doi.org/10.1029/2000wr900328

Tuller, M., Or, D., & Dudley, L. M. (1999). Adsorption and capillary condensation in porous media: Liquid retention and interfacial configurations in angular pores. *Water Resources Research*, *35*(7), 1949–1964. https://doi.org/10.1029/1999wr900098

Turturro, A. C., Caputo, M. C., & Gerke, H. H. (2022). Mercury intrusion porosimetry and centrifuge methods for extended-range retention curves of soil and porous rock samples. *Vadose Zone Journal*, *21*(1), e20176. https://doi.org/10.1002/vzj2.20176

van Genuchten, M. T. (1980). A closed-form Equation for predicting the hydraulic conductivity of unsaturated soils. *Soil Science Society of America Journal*, *44*(5), 892–898. https://doi.org/10.2136/sssaj1980.03615995004400050002x

van Genuchten, M. T., & Nielsen, D. R. (1985). On describing and predicting the hydraulic properties. *Annales Geophysicae*, *3*(5), 615–628.

Vereecken, H., Amelung, W., Bauke, S. L., Bogena, H., Brüggemann, N., Montzka, C., et al. (2022). Soil hydrology in the Earth system. *Nature Reviews Earth and Environment*, *3*(9), 573–587. https://doi.org/10.1038/s43017-022-00324-6

Vereecken, H., Schnepf, A., Hopmans, J. W., Javaux, M., Or, D., Roose, T., et al. (2016). Modeling soil processes: Review, key challenges, and new perspectives. *Vadose Zone Journal*, *15*(5), 1–57. vzj2015-09. https://doi.org/10.2136/vzj2015.09.0131

Vogel, H. J., & Roth, K. (2003). Moving through scales of flow and transport in soil. *Journal of Hydrology*, *272*(1–4), 95–106. https://doi.org/10.1016/s0022-1694(02)00257-3

Wang, Y., Jin, M., & Deng, Z. (2018). Alternative model for predicting soil hydraulic conductivity over the complete moisture range. *Water Resources Research*, *54*(9), 6860–6876. https://doi.org/10.1029/2018wr023037

Wang, Y., Ma, J., & Guan, H. (2016). A mathematically continuous model for describing the hydraulic properties of unsaturated porous media over the entire range of matric suctions. *Journal of Hydrology*, *541*, 873–888. https://doi.org/10.1016/j.jhydrol.2016.07.046

Wang, Y., Ma, J., Guan, H., & Zhu, G. (2017). Determination of the saturated film conductivity to improve the EMFX model in describing the soil hydraulic properties over the entire moisture range. *Journal of Hydrology*, *549*, 38–49. https://doi.org/10.1016/j.jhydrol.2017.03.063

Wang, Y., Ma, J., Zhang, Y., Zhao, M., & Edmunds, W. M. (2013). A new theoretical model accounting for film flow in unsaturated porous media. *Water Resources Research*, *49*(8), 5021–5028. https://doi.org/10.1002/wrcr.20390

Wang, Y., Ma, R., & Zhu, G. (2022). Improved prediction of hydraulic conductivity with a soil water retention curve that accounts for both capillary and adsorption forces. *Water Resources Research*, *58*(4), e2021WR031297. https://doi.org/10.1029/2021wr031297

Wang, Y., Ma, R., & Zhu, G. (2023). Representation of the influence of soil structure on hydraulic conductivity prediction. *Journal of Hydrology*, *619*, 129330. https://doi.org/10.1016/j.jhydrol.2023.129330

Wang, Y., Zhou, J., Ma, R., Zhu, G., & Zhang, Y. (2022b). Development of a new pedotransfer function addressing limitations in soil hydraulic models and observations. *Water Resources Research*, *58*(6), e2021WR031406. https://doi.org/10.1029/2021wr031406

Webb, S. W. (2000). A simple extension of two-phase characteristic curves to include the dry region. *Water Resources Research*, *36*(6), 1425–1430. https://doi.org/10.1029/2000wr900057

Weber, T. K., Durner, W., Streck, T., & Diamantopoulos, E. (2019). A modular framework for modeling unsaturated soil hydraulic properties over the full moisture range. *Water Resources Research*, *55*(6), 4994–5011. https://doi.org/10.1029/2018wr024584

Yang, Z., Li, Z., Tong, X., Hu, S., Wang, J., Ji, S., & Li, L. (2023). Weibull distribution models for describing soil hydraulic properties over the entire matric suction range. *Journal of Hydrology*, *622*, 129661. https://doi.org/10.1016/j.jhydrol.2023.129661

Ye, M., Meyer, P. D., & Neuman, S. P. (2008). On model selection criteria in multimodel analysis. *Water Resources Research*, *44*(3). https://doi.org/10.1029/2008wr006803

Yu, L., & Wardlaw, N. C. (1986). Mechanisms of nonwetting phase trapping during imbibition at slow rates. *Journal of Colloid and Interface Science*, *109*(2), 473–486. https://doi.org/10.1016/0021-9797(86)90325-5

Zhang, Y., Weihermüller, L., Toth, B., Noman, M., & Vereecken, H. (2022). Analyzing dual porosity in soil hydraulic properties using soil databases for pedotransfer function development. *Vadose Zone Journal*, *21*(5), e20227. https://doi.org/10.1002/vzj2.20227

Zhang, Z. F. (2011). Soil water retention and relative permeability for conditions from oven-dry to full saturation. *Vadose Zone Journal*, *10*(4), 1299–1308. https://doi.org/10.2136/vzj2011.0019

Zheng, W., Shen, C., Wang, L. P., & Jin, Y. (2020). An empirical soil water retention model based on probability laws for pore-size distribution. *Vadose Zone Journal*, *19*(1), e20065. https://doi.org/10.1002/vzj2.20065